PBP1 of *Staphylococcus aureus* has multiple essential functions in cell division

Katarzyna Wacnik[1,2], Vincenzo A Rao[3], Xinyue Chen[2,4], Lucia Lafage[1,2], Manuel Pazos[5], Simon Booth[3], Waldemar Vollmer[5], Jamie K Hobbs[2,4], Richard J Lewis[3‡] and Simon J Foster[1,2*]

[1] School of Biosciences, University of Sheffield, Sheffield, UK

[2] The Florey Institute for Host-Pathogen Interactions, University of Sheffield, Sheffield, UK

[3] Biosciences Institute, Newcastle University, Newcastle upon Tyne, UK.

[4] Department of Physics and Astronomy, University of Sheffield, Sheffield, UK

[5] Centre for Bacterial Cell Biology, Bioscience Institute, Newcastle University, Newcastle upon Tyne, UK.

[‡] Current address: The Royal Society for the Protection of Birds, The Lodge, Sandy, Bedfordshire SG19 2DL

* To whom correspondence should be sent. E-mail: s.foster@sheffield.ac.uk.

Abstract

Bacterial cell division is a complex process requiring the coordination of multiple components, to allow the appropriate spatial and temporal control of septum formation and cell scission. Peptidoglycan (PG) is the major structural component of the septum, and our recent studies in the human pathogen *Staphylococcus aureus* have revealed a complex, multi-stage PG architecture that develops during septation. Penicillin binding proteins (PBPs) are essential for the final steps of PG biosynthesis – their transpeptidase activity links together the peptide sidechain of nascent glycan strands together. PBP1 is required for cell division in *S. aureus* and here we demonstrate that it has multiple essential functions associated with its enzymatic activity and as a regulator of division. Loss of PBP1, or just its C-terminal PASTA domains, results in cessation of division at the point of septal plate formation. The PASTA domains can bind PG and thus coordinate the cell division process. The transpeptidase activity of PBP1 is also essential but its loss leads to a strikingly different phenotype of thickened and aberrant septa, which is phenocopied by the morphological effects of adding the PBP1-specific β-lactam, meropenem. Together these results lead to a model for septal PG synthesis where PBP1 enzyme activity is responsible for the characteristic architecture of the septum and PBP1 protein molecules coordinate cell division allowing septal plate formation.

Introduction

Peptidoglycan (PG) is the major structural component of the bacterial cell wall and is essential for maintaining cell shape, integrity and survival (Silhavy et al., 2010; Turner et al., 2014; Vollmer et al., 2008). The final assembly stages of assembly of this large polymeric molecule are mediated by penicillin-binding proteins (PBPs), key PG synthases that, through their transglycosylase (TG) and transpeptidase (TP) activities, polymerise glycan chains and cross-link them into a mesh-like hydrogel (Pasquina-Lemonche et al., 2020; Typas et al.,

2011). Since the cell wall is essential for maintaining bacterial life, PBPs and PG synthesis are a target of some of the most important antibiotics, β-lactams (penicillins) and glycopeptides (vancomycin) (Schneider & Sahl, 2010; Zapun et al., 2008). The major human pathogen *Staphylococcus aureus* has a minimalist PBP system as it encodes only four PBPs, PBP1 to PBP4 (Pinho et al., 2013). Only PBP1 (class B PBP with only TP activity, bPBP) and PBP2 (class A bifunctional PBP with both TG and TP activities, aPBP) are essential and sufficient for septal and peripheral PG synthesis in *S. aureus* (Lund et al., 2018; Pinho et al., 2013). PBP2 is the major PG synthase of *S. aureus*, and the septal formation activity of PBP2 is mediated by its substrate, Lipid II (Pinho & Errington, 2005). Although PBP2 is essential, loss of its TP activity can be compensated for by a horizontally acquired class B PBP2A in methicillin-resistant *S. aureus* (MRSA) (Pinho, Filipe, et al., 2001). PBP2A, however, cannot replace PBP1, whose loss is detrimental to the viability of *S. aureus* (Pereira et al., 2007). PBP1 and PBP3 form cognate pairs with the monofunctional TGs, FtsW and RodA, belonging to the SEDS (shape, elongation, division and sporulation) family (Meeske et al., 2016) to facilitate septum formation (PBP1-FtsW) and to maintain the prolate cell shape (PBP3-RodA) of *S. aureus*, respectively (Reichmann et al., 2019). PBP4 is a class C PBP with D,D-carboxypeptidase activity (cPBP) and has a TP activity that contributes to the high-level cross-linking of PG and MRSA resistance to β-lactams (Loskill et al., 2014; Srisuknimit et al., 2017).

Although *S. aureus* PBPs have been studied over many years, the specific roles of PBP1 in cell division, PG synthesis and architecture have remained elusive. Previous studies have shown that whilst PBP1 is essential, its TP activity is not, implying another role (Pereira et al., 2007; Reichmann et al., 2019). However, this work was performed in an MRSA background that contains PBP2A, encoded by *mecA*, which is non-native to *S. aureus* (Pinho,

de Lencastre, et al., 2001). Whilst PBP2A cannot replace PBP1, how these proteins interact is unknown. We have recently shown that the presence of *mecA* has a profound effect on cellular physiology (Panchal et al., 2020). Thus it is important to understand individual and combined roles of *S. aureus* PBPs both in the presence and absence of the exogenous PBP2A, as the vast majority of *S. aureus* infections are caused by methicillin sensitive strains.

Results

S. aureus PBP1 PASTA domains are essential for growth and PBP1 functionality

PBP1 has a cytoplasmic N-terminal region, a membrane spanning sequence, an exocytoplasmic dimerization domain and a C-terminal region consisting of the TP domain and two PASTA domains (for penicillin-binding protein and serine/threonine kinase associated domain) (Yeats et al., 2002). We created a set of conditional mutants of *pbp1* to investigate the role of PBP1 in cell division and PG synthesis. An ectopic copy of *pbp1* under the control of the P*spac* promoter (P_{spac}-*pbp1*) was placed at the lipase locus (*geh*::P_{spac}-*pbp1*) of *S. aureus* SH1000, and a series of changes were made in this genetic background at the native *pbp1* locus: (i) an in-frame deletion of *pbp1* (Δ*pbp1)*, (ii) a deletion of the region encoding the two PASTA domains (*pbp1*Δ_{PASTA}), and (iii) the substitution of the catalytic Ser314 to Ala in the TP domain (*pbp1**) (Fig. 1a, b). We examined the essentiality of PBP1, the PASTA domains and the active TP domain with these mutants. Depletion of PBP1 via IPTG removal (Fig. 1c and Fig. 1 – figure supplement 1a, b) resulted in cell death, confirming the essentiality of PBP1 (Fig. 1c, d and Fig. 1 – figure supplement 1c, d,). Deletion of the PASTA domains also led to growth inhibition and more than 99% cell death within 4 h (Fig. 1d and Fig. 1 – figure supplement 1c, d). Importantly, this phenotype was not associated with PBP1$_{\Delta PASTA}$ instability (Fig. 1c and Fig. 1 – figure supplement 1a) or loss of its ability to bind its substrate analogue BocillinFL (Fig. 1 – figure supplement 1b). By

93 contrast, deletion of the PASTA domains of *Streptococcus pneumoniae* PBP2x, a PBP1
94 orthologue, resulted in a complete loss of BocillinFL binding (Maurer et al., 2012). These
95 results indicate the PASTA domains are essential for *S. aureus* growth and PBP1
96 functionality but not its enzymatic activity.
97 During construction of the *pbp1** mutant we obtained, by serendipity, a *pbp1*$_{STOP}$ mutant in
98 which a SNP in the codon for Glu292 resulted in its replacement with a premature stop codon
99 and the truncation of the entire TP and PASTAs region of PBP1 (Fig. 1 – figure supplement
100 1e, f). However, immunoblot analysis using anti-PBP1 sera could not confirm the presence of
101 the PBP1$_{STOP}$ protein in the *pbp1*$_{STOP}$ mutant (Fig. 1 – figure supplement 1g), suggesting that
102 stability of the N-terminal domain of PBP1 is dependent on its C-terminus.
103 Although inactivation of PBP1 TP activity (PBP1*) did not affect protein stability (Fig. 1c),
104 it did remove the ability of PBP1 to bind BocillinFL (Fig. 1 – figure supplement 1b). The loss
105 of PBP1 TP activity resulted in severely compromised growth on solid media (Fig. 1d and
106 Fig. 1 – figure supplement 1c) and reduced cellular viability in liquid culture (Fig. 1e and Fig.
107 1 – figure supplement 1d). Thus, the TP activity of PBP1 is required for growth in the
108 SH1000 background. Inactivation of the PBP1 TP activity was reported previously not to
109 affect growth in the COL strain background (Reichmann et al., 2019). The differences in the
110 necessity for the PBP1 TP activity could result from COL being MRSA whereas SH1000 is a
111 methicillin sensitive *S. aureus* (MSSA).
112
113 **PBP1 TP activity is crucial in MSSA but not in MRSA**
114 We have recently developed a set of defined strains where high-level β-lactam resistance of
115 MRSA is mediated by *mecA* encoding PBP2A and a mutation in either *rpoB* or *rpoC*
116 (Panchal et al., 2020). This combination of genetic alterations (*mecA*$^{+}$ *rpoB*) are present in
117 COL (Panchal et al., 2020). To test if the apparent disparity in PBP1 role is associated with

MRSA, we developed a high-level resistant mutant of *pbp1** in the well-characterised *S. aureus* SH1000 by adding the *mecA rpoB*^{H929Q} to the MSSA *pbp1** mutant, resulting in SH1000$_{MRSA}$ *pbp1** (Fig. 1 – figure supplement 2a). Inactivating PBP1 TP did not affect the ability of SH1000$_{MRSA}$ *pbp1** to grow in the absence of IPTG, whereas *pbp1* depletion led to growth inhibition in the isogenic Δ*pbp1* MSSA and MRSA strains (Fig. 1d, e and Fig. 1 – figure supplement 2b-d). Thus, the fundamental role of PBP1 in growth and division can only be studied in an MSSA background as otherwise the role of PBP1 can be confounded by the presence of the MRSA resistance apparatus.

PBP1 PASTA domains are required for septum progression

PG synthesis still occurred in Δ*pbp1*, *pbp1*$_{\Delta PASTA}$ and *pbp1** in the absence of IPTG, despite cell growth inhibition, as measured by the incorporation of the fluorescent D-amino acid derivative HADA (Fig. 2a). This was not a consequence of the non-synthesis, exchange reaction carried out by PBP4 as it occurred in *pbp4* as well as with the dipeptide ADA-DA (Kuru et al., 2019; Lund et al., 2018) (Fig. 2 – figure supplement 1). All variants increased in cell volume upon depletion of *pbp1*, whereas *pbp1*$_{\Delta PASTA}$ was enlarged by almost twice as much as Δ*pbp1* and *pbp1** (Fig. 2a, b and Fig. 2 – figure supplement 2a). Despite differences in cell size, both Δ*pbp1* and *pbp1*$_{\Delta PASTA}$ decreased the number of cells with complete septa (Fig. 2a, c). Transmission electron microscopy (TEM) showed that more than 80% of the population had growth defects including cell wall thickening, PG blebs, mis-shapen and/or multiple, incomplete septa. (Fig 2d, e and Fig. 2 – figure supplement 2b, c). Such septa had abnormally thick bases and sharply pointed leading edges, suggesting that cell growth arrest was not due to a lack of septal initiation but instead arrest of inward septum progression. Atomic force microscopy (AFM) has revealed previously that the first step in cell division is the formation of a PG feature called the “piecrust”, prior to the septal plate(Turner et al.,

2010). The *S. aureus* septal plate has two PG architectures: disordered mesh facing the cell membrane and concentric rings in the septum core (Pasquina-Lemonche et al., 2020). Here lack of PBP1 or the PBP1 PASTA domains led to formation of more than one, and often misplaced, piecrust. These mutations also caused an increase in unfinished septal annuli and alterations in the ring surface architecture (Fig 2f and Fig. 2 – figure supplement 3a, c – arrowheads), a characteristic feature of the division plane, freshly revealed immediately after cell scission (Pasquina-Lemonche et al., 2020). Thus, depletion of PBP1 did not stop septum initiation but the loss of the PASTA domains was enough to cause formation of irregular piecrusts, arrest septal plate formation and lead to an altered septal PG architecture.

PBP1 TP activity regulates septal PG architecture

The *pbp1** mutant gave a novel phenotype quite distinct from loss of entire PBP1 or the PASTA domains. Inactivation of PBP1 TP activity did not prevent initiation and closing of the septa, but instead resulted in accumulation of cells with aberrant septa and separation defects in about 80% of the population (Fig. 2a, c, e). The septa in such cells had a rounded leading edge, were curved, abnormally thick (Fig. 2d, e and Fig. 2 – figure supplement 2b, c), had agglomerations of mesh-like material close to the septal centre in addition to irregular piecrusts as observed by AFM (Fig. 2f and Fig. 2 – figure supplement 3a, b). The intracellular agglomerations are PG as they stain heavily with HADA and ADA-DA (Fig. 2a and Fig. 2 – figure supplement 1c, f) and could be observed in purified sacculi (Fig. 2f and Fig. 2 – figure supplement 3b). No ring architecture, only mesh structured PG could be observed on the surface of the *pbp1** mutant. Importantly, using fluorescence microscopy the *pbp1* pbp3 pbp4* mutant, in which PBP2 is the only active TP, presented a similar phenotype upon IPTG removal as *pbp1**, exemplified by misshapen septa and agglomerations of PG material marked by HADA (Fig. 2 – figure supplement 2d). Therefore, septal synthesis and

progression still occurred in the *pbp1** mutant, however, they resulted from PBP2 transpeptidase activity and potentially the transglycosylase activity of FtsW.

The *pbp1** phenotype occurred specifically because of the loss of the TP activity of this essential enzyme. This phenotype is mirrored by the mode of action of β-lactam antibiotics, which bind to and inhibit the TP activity of PBPs (Schneider & Sahl, 2010). Our results suggest that PBP1 TP activity has a specific role in septal plate formation and without this the septum is mis-shapen. The conditional lethal strains made here allow for functional analysis of the genes concerned. However, phenotypes tend to accumulate on depletion of the wild-type protein over time confusing the precise roles for individual components. To independently corroborate the role of the TP activity of PBP1 we utilized an approach to directly, and selectively, inhibit its activity. Meropenem (MEM) has a higher affinity for PBP1 than PBP2 (Berti et al., 2013; Yang et al., 1995) and, therefore, we hypothesised that its effect on *S. aureus* would match *pbp1**. In a MEM-titration, treatment with 1x MIC MEM was sufficient to lead to cell death and a significant increase in SH1000 WT cell volume after 1 h (Fig. 3a, b and Fig. 3 – figure supplement 1a). More than 70% of MEM treated cells had growth defects that manifested as aberrantly shaped septa and accumulation of PG as shown by HADA labelling (Fig. 3a, c, d Fig. 3 – figure supplement 1c, e), similar to observations made with the *pbp1** mutants (Fig. 2a, c-e, Fig. 2 – figure supplement 1c, f). The MEM phenotype of malformed septa was not linked to PBP3 or PBP4 as it was also observed in the corresponding double mutant (Fig. 3c, d and Fig. 3 – figure supplement 1b, d, f), which corroborated the role of PBP2 in misshapen septal genesis.

PASTA domains mediate PBP1 interaction with division components

The morphologies of the Δ*pbp1* and *pbp1*$_{\Delta PASTA}$ mutants resemble *S. aureus* depleted of DivIB in which EzrA and FtsZ form multiple rings and the synthesis of the cross wall is blocked, despite the normal recruitment of early cell division proteins and piecrust formation (Bottomley et al., 2014). In the Δ*pbp1 ezrA-gfp* mutant, EzrA, which here acts as an early cell division marker, was localised at midcell in the majority of cells and formed additional arcs or rings in 33.5% of the population (Fig. 4a, d). Multiple EzrA rings were observed in 42.7% of the *pbp1*$_{\Delta PASTA}$ *ezrA-gfp* mutant cells (Fig. 4b, d), supporting the requirement for PBP1 PASTA domains for correct selection of the division site. Alternatively, the multiple division rings could result from a lack of the septal progression whereby the unproductive division machinery results in futile additional alternative initiation attempts, suggesting that PASTA domains are involved in the progression from piecrust to septal plate formation. While the number of cells with complete septa (EzrA-GFP visible as a line or focus) reduced by at least 6-fold in Δ*pbp1 ezrA-gfp* and *pbp1*$_{\Delta PASTA}$ *ezrA-gfp*, it only halved in *pbp1* ezrA-gfp* (12.5% to 6.3% of *pbp1* ezrA-gfp* in +/-IPTG, respectively; Fig. 4c, d), confirming that septum progression, although reduced, still occurred when PBP1 TP was inactive implying that TP activity is necessary for correct septal architecture during cell division.

The cell wall of Gram-positive bacteria is decorated with wall teichoic acid (WTA) glycopolymers (Neuhaus & Baddiley, 2003). WTA regulates cell shape, ion homeostasis, autolytic enzymes, growth and division (Swoboda et al., 2010). In *S. aureus*, WTA plays a crucial role in virulence, MRSA resistance to β-lactam antibiotics, PBP4 localisation at the septum and PG cross-linking (Atilano et al., 2010; Campbell et al., 2011; Farha et al., 2013; Weidenmaier et al., 2005). Loss of WTA also results in a proportion of cells with aberrant septa (Campbell et al., 2011) suggesting a link with PBP1 function. Loss of *tarO* (leading to a lack of WTA) caused minor cell division defects in SH1000 (Fig. 4 – figure supplement 1a, e,

f). Combining *tarO* with the mutations in *pbp1* exacerbated the observed morphological defects, with the appearance of distinct septal and off-septal PG foci appeared (marked with HADA) in Δ*pbp1 tarO* and $pbp1_{\Delta PASTA}$ *tarO* (Fig. 4 – figure supplement 1b-f), demonstrating that both WTA and PBP1 are involved in cell cycle control in parallel.

As PBP1 PASTA has a role in the regulation of septal plate formation, this may be determined by interacting with other protein components. In order to examine this hypothesis we performed a bacterial two-hybrid assay, in which PBP1 has previously been found to have multiple interactions (Steele et al., 2011). Truncation of the PASTA domains not only reduced *S. aureus* PBP1 interaction with DivIB but also with FtsW, whilst recognition of other known interacting partners of PBP1 (EzrA, PBP2 and DivIC) were unaffected by the PASTA truncation (Fig. 5 – figure supplement 1a, b), suggesting that these wider interactions involve the N-terminal domain of PBP1.

PBP1 PASTA domains bind peptidoglycan

Impaired interaction with DivIB could be one explanation for why cells depleted of PBP1 PASTA domains initiate irregular piecrusts and septation defects accrue as a consequence. PASTA domains have long been associated with PG binding because of work performed mainly on serine/threonine protein kinases (STPK) (Mir et al., 2011; Shah et al., 2008; Squeglia et al., 2011; Yeats et al., 2002). Therefore, we assessed whether *S. aureus* PBP1 and its PASTA domains could recognise PG by measuring their affinities for *S. aureus* cell wall PG with or without WTA (+/-WTA) with a semi-quantitative fluorescence binding assay (Bottomley et al., 2014) and *S. aureus* PBP1 derivatives produced in *Escherichia coli* (Fig. 5a and Fig. 5 – figure supplement 1c). Both *Sa*PBP1 (K_d 19 ± 4 nM (+WTA), 115 ± 21 nM (-WTA)) and its PASTA domains (*Sa*$PASTA_{PBP1}$; K_d 198 ± 42 nM (+WTA), 109 ± 23 nM (-

242 WTA) bound PG (Fig. 5b). Inactive *Sa*PBP1* was still able to bind PG with a preference for
243 PG with WTA present (K_d 53 ± 8 nM (+WTA), 227 ± 46 nM (-WTA); Fig. 5b), similar to
244 active *Sa*PBP1. Although removal of the PASTA domains did not abolish BocillinFL binding
245 (Fig. 5 – figure supplement 1c), it considerably reduced the ability of *Sa*PBP1$_{\Delta PASTA}$ to bind
246 PG and binding was completely abolished in the presence of WTA (K_d >2000 nM (+WTA),
247 440 ± 57 nM (-WTA); Fig. 5b). By contrast, the PASTA domains (*Sa*PASTA$_{PBP1}$) on their
248 own bind to *S. aureus* PG but are incapable of binding BocillinFL (Fig. 5b and Fig. 5 – figure
249 supplement 1c). These results demonstrate unequivocally that PBP1 is a PG binding protein,
250 and the PASTA domains have a dominant role in this interaction. Sequence conservation
251 analysis of PASTA domains revealed the presence of either Arg or Glu residues in
252 classifying a PASTA domain as a PG-binder (Calvanese et al., 2017). The PASTA domains
253 of *S. aureus* PBP1 each have proline at the equivalent positions (residues Pro603 and Pro661)
254 and thus PBP1 would be predicted as a non-PG binder, which clearly is not the case from the
255 experimental evidence presented herein. Not only have we demonstrated the existence of
256 such an interaction but we have also quantified it, suggesting that the predicted significance
257 of conserved Arg or Glu residues with regard to PG binding is either only relevant to PASTA
258 domains found in STPKs, linear arrangements of tandem PASTA repeats, or is too simplistic
259 a prediction for proteins with multiple and complex functions like PBPs.
260

261 To gain a better understanding of the role of the PASTA domains in *S. aureus* PBP1
262 (*Sa*PASTA$_{PBP1}$), we determined their structure by X-ray crystallography. Soluble
263 recombinant protein was obtained in high yield from the cytoplasm of *E. coli* cells and well-
264 ordered crystals were subsequently produced that diffracted to a maximum resolution of 1.78
265 Å (Appendix Table 4). The structure was solved by molecular replacement using the
266 corresponding PASTA domains present in *Sp*PBP2x from PDB entry 5OAU (Bernardo-

García et al., 2018), which shares 26% sequence identity with *Sa*PASTA$_{PBP1}$. The asymmetric unit contains two monomers (labelled A and B), each forming a 2-layer sandwich comprising an α-helix and a three-stranded antiparallel β-sheet, distinct from the TP domain (Fig. 5c). Clear and continuous electron density allowed the modelling and unambiguous assignment of both PASTA domains (Fig. 5c). When *Sa*PASTA$_{PBP1}$ is compared with other structures deposited in the PDB using *DALI* (Holm, 2020), the top hit identified was *S. pneumoniae* PBP2x (Z-score; 15.7), showing a significant conservation of the PASTA fold, despite low sequence identity (Fig. 5c). Unlike the linear arrangement observed for PASTA domains in serine/threonine kinases (Barthe et al., 2010; Ruggiero et al., 2011), *Sa*PASTA$_{PBP1}$ adopts a compact upside-down globular arrangement (Fig. 5c). The arrangement of the two PASTA domains solved here, in isolation from the TP domain in comparison to structural analyses of *Sp*PBP2x, is entirely consistent with a non-linear PASTA domain arrangement. First, the structures of *Sa*PASTA$_{PBP1}$ and the PASTA domains of *Sp*PBP2x share a pairwise RMSD of 2.2 Å over 114 Cα and when *Sa*PASTA$_{PBP1}$ is superimposed on the PASTA domains of *Sp*PBP2x there are no steric clashes with the TP domain. Second, the linker between PASTAs in *Sa*PASTA$_{PBP1}$ has a sequence of DGDLTMPDMSGW, is neither glycine- nor alanine-rich, is not predicted to be disordered using IUPred2 or ANCHOR2 webservers and has a mean B factor of 44 Å^2 in comparison to a mean B factor of 42 Å^2 for the entire chain. Third, the interface between the PASTA domains is more reminiscent of the hydrophobic core of a globular protein than the more polar interface observed between molecules in crystal packing. It would therefore seem unlikely that the two PASTA domains open and close in a hinged manner, akin to the movement of a butterfly's wings, in the presence and absence of endogenous PG. Finally, the two proline residues that apparently define PBP1 as a non-binder of PG are found buried from solvent either at the interface of PASTA domain 1 with the TP domain (Pro603) or at the interface between the TP domain and PASTA domains 1 and 2

(Pro661). This latter interface includes the only tryptophan (Trp666) in the sequence of *Sa*PASTA$_{PBP1}$; tryptophan residues are frequent 'markers' of carbohydrate binding sites in proteins (Hudson et al., 2015) and in the absence of any obvious grooves or surface features associated with conserved sequence distributions and/or electrostatics it remains unclear how the PASTA domains of *Sa*PBP1 recognise PG.

Discussion

S. aureus has just two essential PBPs (Reed et al., 2015) and so forms an apparently simple system to understand cell wall growth and division. Even the transpeptidase activity of these two enzymes can be substituted by a single enzyme in the presence of β-lactam antibiotics via the acquisition of PBP2A, encoded by *mecA*, in MRSA strains. Our recent study has revealed that the presence of *mecA* and associated genetic lesions have a profound effect on *S. aureus,* even in the absence of antibiotics (Panchal et al., 2020), leading to the discovery herein that the PG biosynthetic activity of PBP1 is essential in MSSA but not in MRSA (Fig. 1d). This observation has important ramifications for many studies in *S. aureus* where the use of an MRSA background can complicate phenotype interpretation. To understand the fundamental role of PBP1 activity in basic cell physiology we have thus used a MSSA strain with a defined genetic background.

The essential function of PBP1 is associated with its crucial role in septal PG synthesis (Pereira et al., 2009; Reichmann et al., 2019). Here we show that PBP1 is a multifunction regulatory and PG synthetic protein involved in both early and later stages of septum synthesis. PBP1 can interact with other cell division components, make and bind to PG. PG binding is primarily mediated by the PASTA domains that are essential for cell division. There is clear overall structural similarity between *S. aureus* PBP1 and *S. pneumoniae* PBP2x

317 PASTA domains in the way that the two tandem PASTA domains associate into an anti-
318 parallel bundle (Fig. 5c); this is in marked contrast to the head-to-tail linear PASTA domain
319 repeats more typically found in STPKs. The highly hydrophobic interface between the two
320 PASTA domains means it is unlikely to open up like butterfly wings to bind to PG; similarly
321 an extensive, linear interaction with PG, which is likely to occur with the head-to-tail PASTA
322 domain arrangements seen in STPKs and that may require their dimerization (Barthe et al.,
323 2010), does not occur in *Sa*PBP1. Despite the successful production of diffracting crystals of
324 *Sa*PASTA$_{PBP1}$ grown in the presence of PG fragments (including an *N*-acetylglucosamine:*N*-
325 acetylmuramic acid disaccharide) none of the structures yielded electron density features
326 consistent with the stable binding of PG fragments. There are several potential explanations,
327 including a lack of affinity of PASTA domains for small PG fragments, unrepresentative of
328 the sacculus of *S. aureus*; our sedimentation assay does not permit the analysis of the binding
329 of PASTA domains to small, soluble PG precursors. Consequently, and in common with all
330 other PASTA domain structural analyses, the molecular details of PG recognition by *Sa*PBP1
331 remain elusive.
332
333 *S. aureus* is a spheroid coccus that can divide successively in three orthogonal planes
334 (Saraiva et al., 2020; Turner et al., 2010). Septation is first observed as the formation of a
335 thick band of PG known as the piecrust (Turner et al., 2010). This then transitions to the
336 production of the septal plate itself, an initially V-shaped structure with a narrower leading
337 edge (Lund et al., 2018). After closure of the septal annulus, the now bowed septum fills out
338 to yield the mature structure prior to septal scission. The septal plate has two distinct PG
339 architectures with a ring-like pattern at its core, which is exposed upon scission, and a
340 subsequently-synthesised fine mesh, akin to the rest of the peripheral cell wall (Pasquina-
341 Lemonche et al., 2020). Loss of the entire PBP1, or just its PASTA domains, does not

prevent piecrust formation but does result in multi- and/or off-centre piecrusts without the ability to produce the septal plate (Fig 2f). Thus, piecrust formation does not require PBP1 but is likely the result of the activity of the essential PBP2. PBP1 may regulate division site selection through PG cell wall recognition via its PASTA domains. Alternatively, as the division apparatus is unable to progress effectively to septal plate formation due to the lack of PBP1, this may lead to further rounds of initiation and piecrust formation. PBP1 has a clear role in septal plate formation where in the absence of PBP1 or the PASTA domains, cells form aberrantly shaped septa that do not close their annuli (Fig. 2a-e). In stark contrast, inactivation of PBP1 TP activity (*pbp1**) does not stop inward septum progression as observed with loss of PBP1 or the PASTA domains, however, such septa are mis-shapen, curved and abnormally thick (Fig. 2a-e and Fig. 3). The use of the PBP1-specific antibiotic MEM at 1x MIC led to the similar morphology of thickened and mis-shapen septa. Two independent avenues of research both lead to the conclusion that PBP1 TP activity is essential and, whilst septum formation is disturbed, it is not entirely prevented. Therefore PBP1 retains its regulatory function(s) regardless of activity loss. As well as binding to the cell wall, PBP1 also interacts with multiple protein partners including EzrA, DivIB/C, PBP2 and FtsW (Fig. 5 – figure supplement 1a, b) (Steele et al., 2011; Reichmann et al., 2019). Recently, the PASTA domains from *B. subtilis* PBP2B were shown to regulate PBP2B interaction with DivIB (Morales Angeles et al., 2020). *S. aureus* DivIB is a PG binding protein essential for division, which depletion leads to septal plate formation loss (Bottomley et al., 2014; Steele et al., 2011)[9]. Here the PBP1 PASTA domains were found to bind DivIB and FtsW, alluding to their essential role in cell division. FtsW is a SEDS protein, whose TG activity requires the presence of PBP1 (Taguchi et al., 2019). Bifunctional aPBPs (including PBP2) and bPBP-SEDS (including PBP1-FtsW) pairs share similar activities but the fact they coexist in many bacterial species implies there is a division of responsibilities between them.

Indeed, it has been proposed lately that bPBP-SEDS pairs likely lay the primary PG matrix, while aPBPs support the initial PG by modifying, filling in and adding PG to it (Cho et al., 2016; Straume et al., 2020). The *S. aureus* septal plate PG has two distinct architectures, a disordered mesh present on its cytoplasm facing side and a ring structure at its core, which is revealed after the cells have split (Pasquina-Lemonche et al., 2020; Turner et al., 2010) (Fig. 5 – figure supplement 2). Recent AFM analysis from *Staphylococcus warneri* also describes the distinct PG architectures during septation as piecrust and septal plate rings/mesh (Su et al., 2020) . When sacculi are purified from *S. warneri*, the septum can split apart revealing the rings, even in septa that have not closed their annulus, showing that the rings are not a result of PG hydrolysis during cell scission. We hypothesise (Fig. 5 – figure supplement 2) that once the piecrust has been produced, PBP1 and FtsW use this as a foundation to initiate septal plate formation. Together they make the rings of material that become the core of the developing septum, providing the framework for PBP2 to make the bulk of the septal plate as a tight mesh alongside PBP4 and the insertion of WTA via the *tar* pathway. Loss of PBP1 TP activity in the presence of active PBP2 leads to the lack of the ring framework and aberrant, unproductive septum formation. The rings that form the centre of the developing septum also provide the cleavage plane during scission.

Cell division is a fundamental requirement for life. A central question to this in bacteria is how is the division septum synthesised and then split to yield two daughter cells whilst maintaining cellular integrity in the face of internal turgor? Here we have begun to answer this question by revealing the complex synthesis coordination mechanisms that allow this biological engineering feat to be accomplished.

Materials and methods

Bacterial growth conditions

Strains used in this study are listed in Appendix Table 1.

All *Staphylococcus aureus* strains were grown in tryptic soy broth (TSB) containing appropriate antibiotics at 37°C, unless otherwise indicated, with aeration.

All *Escherichia coli* strains, unless otherwise stated, were grown in Lysogeny broth (LB) containing appropriate antibiotics at temperatures ranging from 20°C to 37°C with aeration. For solid media 1.5% (w/v) agar was added.

When necessary, growth medium was supplemented with kanamycin (50 μg ml^{-1}), tetracycline (1 μg ml^{-1}), chloramphenicol (10 μg ml^{-1}, *S. aureus*; 30 μg ml^{-1}, *E. coli*), erythromycin (5 μg ml^{-1}), spectinomycin (250 μg ml ml^{-1}), ampicillin (100 μg ml^{-1}), meropenem (0.4 μg ml^{-1}, 1x MIC for SH1000 WT; 0.2 μg ml^{-1}, 1x MIC for *pbp3 pbp4*), 5-bromo-4-chloro-3-indolyl β-d-thiogalactopyranoside (X-Gal; 80 μg ml^{-1}, *S. aureus*; 40 μg ml^{-1}, *E. coli*) or isopropyl β-d-thiogalactopyranoside (IPTG, 50 μM or 1 mM).

Plasmid construction

Plasmids and oligos used in this study are listed in Appendix Table 2 and Appendix Table 3, respectively.

Plasmids were cloned using *E. coli* NEB5α following previously described methods (Gibson et al., 2009; Sambrook et al., 1989).

pKB-P*spac-pbp1*

A fragment containing RBS and coding region of *S. aureus pbp1* was PCR amplified from the genomic DNA of *S. aureus* SH1000 using pCQ-pbp1-F/-R primers and cloned into NheI and AscI cut pCQ11-FtsZ-SNAP by Gibson assembly, resulting in pCQ11-P*spac-pbp1*. Next

the region containing P*spac*, RBS and *pbp1* was PCR amplified from pCQ11-P*spac-pbp1* using pKB-Pspac-pbp1-F/-R primers and cloned into BamHI and EcoRI cut pKASBAR by Gibson assembly giving pKB-P*spac-pbp1*.

pMAD-Δ*pbp1*

Fragments encompassing 1 kb regions flanking upstream (from -980 bp upstream of *pbp1* to first 20 bp of *pbp1*) and downstream of (from 2214 bp of *pbp1* to 970 bp downstream of *pbp1*) *pbp1* were PCR amplified from *S. aureus* SH1000 genomic DNA using primer pairs pbp1-A/-B and pbp1-C/-D, respectively, and cloned into BamHI and EcoRI cut pMAD by Gibson assembly, creating a deletion vector pMAD-Δ*pbp1*.

pMAD-*pbp1*$_{\Delta PASTA}$

Fragments encompassing 1.5 kb regions flanking the region encoding *pbp1* PASTA domains (upstream, from 286 bp to 1785 bp of *pbp1*; downstream, from 2214 bp of *pbp1* to 970 bp downstream of *pbp1*) were PCR amplified from *S. aureus* SH1000 genomic DNA using pbp1-E/-F and pbp1-G/-H primers and cloned into BamHI and EcoRI cut pMAD by Gibson assembly, resulting in a deletion vector pMAD-*pbp1*$_{\Delta PASTA}$.

pMAD-*pbp1**

A ~1.3 kb fragment covering an upstream region of the active site of *pbp1* (from -334 bp upstream of *pbp1* to first 950 bp of the *pbp1* coding sequence), and a ~1.3 kb fragment comprising the 3′ fragment of *pbp1* (930-2235 bp region of *pbp1*) were PCR amplified from *S. aureus* SH1000 genomic DNA using primer pairs pbp1*5′-F/-R and pbp1*3′-F/-R, respectively. Primers pbp1*5′-R and pbp1*3′-F were designed to introduce a T to G point

mutation resulting in a Ser314Ala substitution. The PCR products were ligated with pMAD cut with EcoRI and BamHI by Gibson assembly, resulting in pMAD-*pbp1**.

T25-PBP1$_{\Delta PASTA}$

A fragment encoding *S. aureus pbp1* without the PASTA domains (M1-S595) was PCR amplified from *S. aureus* SH1000 genomic DNA using T25-pbp1-F and T25-pbp1pasta-R and cloned into BamHI and EcoRI cut pKT25, resulting in T25-PBP1$_{\Delta PASTA}$.

pVR plasmids

Full-length *pbp1* (M1-D744) was *E. coli* codon optimised, synthesised by GenScript, PCR amplified using VR47F/R and cloned into KpnI and HindIII cut pOPINRSF using In-Fusion cloning (Takara Bio), resulting in pVR01. Construction of pVR02 (*Sa*PBP1, M37-D744) and pVR06 (*Sa*PASTA$_{PBP1}$, S595-D744) was performed using inverse PCR (iPCR) (Erster & Liscovitch, 2010), pVR01 as a template and primer pairs VR49F/VR49R and VR57F/VR49R, respectively. pVR03 (*Sa*PBP1*, M37-D744, S314A) and pVR04 (*Sa*PBP1$_{\Delta PASTA}$, M37-S595), were constructed by QuikChange Site-Directed Mutagenesis of pVR02 using VR51 and VR53, respectively.

pSA50

In order to construct an overexpression plasmid for sPBP1-BAP, A51-D744 fragment of *E. coli* codon optimised *pbp1* was PCR amplified using primers OPPF20018F/OPPF20018R and cloned into KpnI and SfoI cut pOPINJB by In-Fusion cloning (Takara Bio). The resulting construct, pSA50 contains an N-terminal hexahistidine-tag fused to Glutathione-S-transferase followed by a Human Rhinovirus 3C protease site, while the PBP1 (A51-D744) C-terminal end is fused to a Biotin Acceptor Peptide (BAP) sequence.

464

465 **Construction of *S. aureus* mutants**

466 All vectors were passed through a restriction-deficient *S. aureus* RN4220 before being
467 transduced into a final *S. aureus* SH1000 strain. Transformation and phage transduction of *S.*
468 *aureus* were carried out as described previously (Novick & Morse, 1967; Schenk & Laddaga,
469 1992).

470

471 **Δ*pbp1*, *pbp1*$_{\Delta PASTA}$ and *pbp1**

472 For construction of *pbp1* mutation strains, first an ectopic copy of *pbp1* under the control of
473 the P*spac* promoter was introduced at the lipase (*geh*) locus. Electrocompetent CYL316 was
474 transformed with pKB-P*spac-pbp1*. The chromosomal fragment containing the integrated
475 plasmid was moved into *S. aureus* SH1000 by phage transduction, resulting in SJF4588 (*S.*
476 *aureus* SH1000 *geh::*P*spac-pbp1*). Next electrocompetent RN4220 was transformed with
477 pMAD-Δ*pbp1*, pMAD-*pbp1*$_{\Delta PASTA}$ or pMAD-*pbp1** and the plasmids were moved to
478 SJF4588 by phage transduction. Integration at 42°C and excision at 28°C of pMAD-Δ*pbp1*,
479 pMAD-*pbp1*$_{\Delta PASTA}$ or pMAD-*pbp1**, resulted in strains SJF5116, SJF5275 and SJF4590,
480 respectively. To allow controlled expression of *pbp1* from P*spac*, pGL485, a multi-copy
481 plasmid carrying *lacI*, was introduced creating strains Δ*pbp1* (*S. aureus* SH1000 *geh::*P*spac-*
482 *pbp1* Δ*pbp1 lacI*), *pbp1*$_{\Delta PASTA}$ (*S. aureus* SH1000 *geh::*P*spac-pbp1 pbp1*$_{\Delta PASTA}$ *lacI*) and
483 *pbp1** (*S. aureus* SH1000 *geh::*P*spac-pbp1 pbp1* lacI*).

484

485 **MRSA Δ*pbp1* and MRSA *pbp1***

486 In order to construct high-level β-lactam resistant mutants, Δ*pbp1* and *pbp1** were
487 transformed with a phage lysate from SJF5046 (*S. aureus* SH1000*lysA::*p*mecA rpoB*^{H929Q})
488 with selection for erythromycin resistance, resulting in low-level β-lactam resistant Δ*pbp1*

p*mecA* and *pbp1** p*mecA*. The low-level resistant mutants were transduced again with the phage lysate from SJF5046 and selected for kanamycin resistance, resulting in MRSA Δ*pbp1* (*S. aureus* SH1000 *geh::*P*spac-pbp1* Δ*pbp1 lacI lysA::*p*mecA rpoB*^{H929Q}) and MRSA *pbp1* pbp1* (*S. aureus* SH1000 *geh::*P*spac-pbp1 pbp1* lacI lysA::*p*mecA rpoB*^{H929Q}). MIC values were determined using antibiotic susceptibility tests using E-test M.I.C. Evaluator (Oxoid) strips.

pbp3 pbp4

SH1000 was transduced with a phage lysate from NE420 (*S. aureus* JE2 *pbp3::Tn*) resulting in SH4421 (*S. aureus* SH1000 *pbp3::Tn*). To swap the erythromycin resistance cassette to a kanamycin cassette, SH4425 (*S. aureus* SH1000 *pbp4::Tn*) was transduced with a phage lysate from NE3004 (*S. aureus* RN4220 pKAN). Integration at 42°C and excision at 28°C of pSPC resulted in strain SH5115 (*S. aureus* SH1000 *pbp4::kan*). SH4421 was subsequently transduced with a phage lysate from SH5115 (*S. aureus* SH1000 *pbp4::Tn*) resulting in *pbp3 pbp4* (SH5483; *S. aureus* SH1000 *pbp3::Tn pbp4::kan*).

Δpbp1 pbp4, pbp1*$_{\Delta PASTA}$ *pbp4* and *pbp1* pbp4

Δ*pbp1, pbp1*$_{\Delta PASTA}$ and *pbp1** were transduced with a phage lysate from SH5115 (*S. aureus* SH1000 *pbp4::kan*), resulting in Δ*pbp1 pbp4* (*S. aureus* SH1000 *geh::*P*spac-pbp1* Δ*pbp1 lacI pbp4::kan*), *pbp1*$_{\Delta PASTA}$ *pbp4* (*S. aureus* SH1000 *geh::*P*spac-pbp1 pbp1*$_{\Delta PASTA}$ *lacI pbp4::kan*) and *pbp1* pbp4* (*S. aureus* SH1000 *geh::*P*spac-pbp1 pbp1* lacI pbp4::kan*), respectively.

pbp1* pbp3 pbp4

513 *pbp1* pbp4* (*S. aureus* SH1000 *geh::*P*spac-pbp1 pbp1* lacI pbp4::kan*) was transduced with
514 a phage lysate from SH4421 (*S. aureus* SH1000 *pbp3::Tn*), resulting in *pbp1* pbp3 pbp4* (*S.*
515 *aureus* SH1000 *geh::*P*spac-pbp1 pbp1* lacI pbp3::Tn pbp4::kan*)**.**
516
517 **Δ*pbp1 ezrA-gfp, pbp1*$_{\Delta PASTA}$ *ezrA-gfp* and *pbp1* ezrA-gfp***
518 Δ*pbp1, pbp1*$_{\Delta PASTA}$ and *pbp1** were transduced with a phage lysate from JGL227 (*S. aureus*
519 SH1000 *ezrA-gfp*+), resulting in Δ*pbp1 ezrA-gfp* (*S. aureus* SH1000 *geh::*P*spac-pbp1* Δ*pbp1*
520 *lacI ezrA-gfp*), *pbp1*$_{\Delta PASTA}$ *ezrA-gfp* $_{PASTA}$ (*S. aureus* SH1000 *geh::*P*spac-pbp1 pbp1*$_{\Delta PASTA}$
521 *lacI ezrA-gfp*) and *pbp1* ezrA-gfp* (*S. aureus* SH1000 *geh::*P*spac-pbp1 pbp1* lacI ezrA-gfp*),
522 respectively**.**
523
524 **Δ*pbp1 tarO, pbp1*$_{\Delta PASTA}$ *tarO* and *pbp1* tarO***
525 Δ*pbp1, pbp1*$_{\Delta PASTA}$ and *pbp1** were transduced with a phage lysate from *tarO tarO*+ (*S.*
526 *aureus* SA113 Δ*tarO::ery* pUC1-*tarO*), resulting in Δ*pbp1 tarO* (*S. aureus* SH1000
527 *geh::*P*spac-pbp1* Δ*pbp1 lacI* Δ*tarO::ery*), *pbp1*$_{\Delta PASTA}$ *tarO* $_{PASTA}$ (*S. aureus* SH1000
528 *geh::*P*spac-pbp1 pbp1*$_{\Delta PASTA}$ *lacI* Δ*tarO::ery*) and *pbp1* tarO* (*S. aureus* SH1000
529 *geh::*P*spac-pbp1 pbp1* lacI* Δ*tarO::ery*), respectively**.**
530
531 **PBP1 depletion**
532 P*spac-pbp1* strains were grown from an OD_{600} of 0.1 to exponential phase (OD_{600} ~ 0.5) in
533 TSB containing 10 μg ml^{-1} chloramphenicol and 50 μM IPTG. Cells were washed three
534 times by centrifugation and resuspension in TSB. Washed cells were then used to inoculate
535 TSB 10 μg ml^{-1} chloramphenicol. Cultures were inoculated to an OD_{600} 0.05 for phenotypic
536 studies and an OD_{600} 0.005 for growth studies. For phenotypic analysis, cultures were
537 incubated for 2 h to allow depletion of PBP1 before microscopy imaging. Control samples

were grown in TSB supplemented with 10 µg ml^{-1} chloramphenicol and 1 mM (50 µM, *ezrA-gfp* mutants) IPTG.

For the plating efficiency test, cells grown in the presence of 10 µg ml^{-1} chloramphenicol and 50 µM IPTG to exponential phase (OD_{600} ~ 0.5) were washed three times in PBS. Serial dilutions of washed cells were plated on TSB 10 µg ml^{-1} chloramphenicol with or without 1 mM IPTG. Relative plating efficiency ($\%CFU$) is expressed as the number of cells that grow on plates without IPTG ($CFU_{no\ IPTG}$) to cells that grow in the presence of IPTG (CFU_{IPTG}) multiplied by 100%:

$$\%CFU = \frac{CFU_{no\ IPTG}}{CFU_{IPTG}} \times 100\%$$

Meropenem activity assays

S. aureus strains were grown overnight in TSB. The overnight cultures were used to inoculate fresh TSB media to an OD_{600} of 0.05. When cells reached an OD_{600} of 0.2-0.4, meropenem was added, and the change of bacterial count was monitored. The colony-forming units per ml of culture (CFU/ml) measures were normalized to the initial CFU/ml at the time of the antibiotic addition, at time zero (t_0).

$$Relative\ CFU/ml = \frac{CFU/ml_{tn}}{CFU/ml_{t0}}$$

For phenotypic analysis, cells were treated for 1 h with 1x MIC meropenem before microscopy imaging.

Fractionation of *S. aureus* membranes

The membrane fraction of *S. aureus* was prepared as previously described (García-Lara et al., 2015) with the following modifications. *S. aureus* cells grown to the appropriate growth phase were recovered by centrifugation (5,000 x g, 10 min, 4°C), washed three times by

562 resuspension and centrifugation (5,000 x g, 10 min, 4°C) in PBS. Cells were resuspended in
563 TBSI and broken using 0.1 mm silica spheres (Lysing Matrix B) and FastPrep Homogenizer
564 (MP Biomedicals) in 12 cycles of 30 s, at maximum speed (6.5 m s^{-1}), with 5 min incubation
565 on ice between cycles. Cell lysates were centrifuged (5,000 x g, 10 min, 4°C) to remove
566 unbroken cells. The supernatant was then spun (5,000 x g, 10 min, 4°C) to sediment cell wall
567 material. The membrane fraction was recovered from the supernatant by centrifugation
568 (35,000 x g, 20 min, 4°C) and the pellet (membranes) was resuspended in PBS. The total
569 protein concentration was estimated by Bradford assay.
570
571 ***In vitro* labelling of *S. aureus* PBPs with BocillinFL**
572 This method was adopted from a published protocol (Zhao et al., 1999) with minor
573 modifications. Membrane proteome samples (25 µg in 20 µl PBS) and purified proteins (2.5
574 µg in 25 µl HEPES pH 7.5 150 mM NaCl) were incubated with 25 µM BocillinFL
575 (Invitrogen) for 20 min at 37°C. Additionally for competition assay, purified *Sa*PBP1 was
576 mixed with 2.5 µg (~286 µM final concentration) ampicillin and incubated at 37˚C for 10
577 min prior to the addition of BocillinFL. The reaction was stopped by the addition of 5x SDS-
578 PAGE loading buffer. Membrane proteome was additionally incubated for 10 min at 90°C.
579 The samples were run on a 6-20% (w/v) SDS-PAGE gradient or 10% (w/v) SDS-PAGE gel
580 and visualized using a BioRad ChemiDoc MP Imaging system or a GE Typhoon FLA 9500.
581
582 **Labelling *S. aureus* DAAs**
583 *S. aureus* cells were incubated with 500 µM (2 mM for *pbp4* mutants) HADA or 1 mM
584 ADA-DA at 37°C for 5 min. Cells were then washed by centrifugation and resuspension in
585 PBS.
586

Click chemistry

ADA-DA containing an azide functional group was fluorescently labelled with Alexa Fluor 488 Alkyne at 5 μg ml^{-1} via the Click reaction (copper (I)-catalysed alkyne-azide cycloaddition). This was carried out using the Click-iT Cell Reaction Buffer Kit (ThermoFisher) according to the manufacturer's protocol.

Labelling *S. aureus* with fluorescent NHS-ester

Fixed cells wells were resuspended in PBS containing 8 μg ml^{-1} Alexa Fluor 555 NHS ester (Invitrogen) and incubated at room temperature for 30 min. Cells were washed twice by centrifugation and resuspension in PBS.

Fixing for fluorescence microscopy

Cells were fixed by incubation in 1.6% (w/v) paraformaldehyde at room temperature for 30 min.

Fluorescence microscopy

Fixed cells were dried onto a poly-l-Lysine coated slide, mounted in PBPS and imaged on a Nikon Ti Inverted microscope fitted with a Lumencor Spectra X light engine. Images were taken using a 100x PlanApo (1.4 NA) oil objective using 1.518 RI oil and detected by an Andor Zyla sCMOS camera.

Cell volume estimation

Cell volume calculations were carried out as previously described (Zhou et al., 2015). The long and short axis of cells were measured using Fiji. The volume was then calculated based on a prolate spheroid shape with volume:

612 $$V = \frac{4}{3}\pi ab^2,$$

613 where *a* and *b* are the radii along the long and short axis, respectively.

614

615 **Transmission electron microscopy**

616 *S. aureus* strains were prepared for electron microscopy as previously described (Sutton et

617 al., 2021).

618

619 **Preparation of *S. aureus* sacculi**

620 Peptidoglycan from *S. aureus* cells was extracted and if required HF treated to remove cell

621 wall polymers as previously described (Sutton et al., 2021).

622

623 **Sacculi immobilisation for AFM Imaging**

624 Immobilisation surface was prepared by adding the solution mixed by 171 µL 100 mM

625 $NaHCO_3$, 3 µl of 1 M NaOH and 6 µl of Cell-Tak (Corning, 5% (w/v) in acetic acid) on

626 freshly cleaved mica. After 30 min incubation, the surface was washed by 5 × 200 µl HPLC

627 grade water. Sacculi stocks were 10 times diluted in HPLC grade water and briefly tip-

628 sonicated to re-suspend in prior to immobilisation. 10 µl of the sacculi suspension was added

629 to 40 µl of HPLC grade water on the Cell-Tak immobilisation surface and incubated for 1 h.

630 The surface was then thoroughly rinsed with HPLC grade water, blow-dried with nitrogen

631 and stored in petri-dish at room temperature before AFM imaging.

632

633 **AFM Imaging and image analysis**

634 AFM imaging was carried out on a Nanowizard III ULTRA Speed system (JPK, Germany).

635 Rectangular cantilevers with nominal spring constant of 0.3 N/m and resonant frequency (in

636 liquid) of ~ 150 kHz (USC-F0.3-k0.3, NanoWorld, Switzerland) were used. The spring

637 constant and deflection sensitivity of each cantilever was calibrated prior to each
638 measurement (Hutter & Bechhoefer, 1993; Sader et al., 2016) Measurements were carried out
639 in Quantitative Imaging mode at room temperature, in the buffer composed of 200 mM KCl
640 and 10 mM Tris. Scans were driven at a line rate of ~ 0.78 Hz, with a typical Z length of 300
641 nm and trigger force of 20 nN.
642 Resultant topographic images were processed using JPK Data Processing. No flattening or
643 surface subtraction was applied. High pass filter (scale: 100% to 500%, degree of smoothing:
644 5 px, horizontal) was applied to the higher magnification images to enhance the contrast
645 without modifying the morphological features. The morphological features of sacculi were
646 summarised from images obtained on abundant technical repeats of 2 biological replicates.
647
648 **Recombinant protein production and purification**
649 **sPBP1-BAP**
650 *E. coli* BL21(DE3) cells containing plasmid pSA50 were grown in LB medium supplemented
651 with 100 µg ml^{-1} ampicillin at 37°C to an OD_{578} of 0.5. Protein overproduction was induced
652 by addition of 0.5 mM IPTG to the cell culture and further incubation for 4 h at 30°C. Cells
653 were harvested by centrifugation (6,200 x g, 15 min, 4°C) and the pellet was resuspended in
654 basic buffer (25 mM Tris-HCl, 100 mM NaCl, pH 7.5). After addition of 1 mM PMSF,
655 1:1,000 dilution of protease inhibitor cocktail (Sigma-Aldrich) and DNase, the cells were
656 disrupted by sonication (Branson Digital Sonifier). The cell lysate was centrifuged (130,000
657 x g, 60 min, 4°C) and the supernatant was recovered. The supernatant was incubated with Ni-
658 NTA Superflow (Qiagen) for 2 h at 4°C with gentle stirring, which had been pre-equilibrated
659 in basic buffer. The resin was poured into a gravity column and washed with 20 volumes of
660 wash buffer (25 mM Tris-HCl, 150 mM NaCl, 10% (v/v) glycerol, 10 mM $MgCl_2$, 20 mM
661 imidazole, pH 7.5). Bound protein was eluted with elution buffer (25 mM Tris-HCl, 150 mM

NaCl, 10% (v/v) glycerol, 10 mM $MgCl_2$, 600 mM imidazole, pH 7.5). 10 U ml−1 of HRV-3C protease (Takara) were added to the Ni-NTA eluted protein to remove the oligohistidine-GST-tag during dialysis against 3 L of dialysis buffer I (25 mM Tris-HCl, 150 mM NaCl, 10 mM EGTA, 10% (v/v) glycerol, pH 7.5) for 20 h at 4°C. Digested protein was dialysed against 3 L of dialysis buffer II (25 mM Tris-HCl, 150 mM NaCl, 10 mM $MgCl_2$, 10% (v/v) glycerol, pH 7.5), for 3 h at 4°C. The protein was incubated in the same Ni-NTA beads (pre-equilibrated in dialysis buffer II) for 2 h at 4°C to remove the contaminants and the His-GST tag from the sample. The flow through and the washes (2 volume of wash buffer) were pooled, dialysed against storage buffer (25 mM HEPES-NaOH, 150 mM NaCl, 10 mM $MgCl_2$, 10% (v/v) glycerol, pH 7.5) and concentrated using a Vivaspin Turbo 15 column (MWCO 50000 Da).

_Sa_PBP1, _Sa_PBP1*, _Sa_PBP1$_{\Delta PASTA}$ and _Sa_PASTA$_{PBP1}$

All recombinant proteins were produced in *E. coli* Rosetta (DE3) cells at 37°C in TB medium supplemented with 50 µg ml^{-1} kanamycin and 30 µg ml^{-1} chloramphenicol. Once cultures had reached OD_{600} 0.9, protein expression was induced with 1 mM IPTG for 20 h at 20°C. Cells were harvested by centrifugation (4,000 x g at 4°C for 30 mins) and the pellet was resuspended in a buffer of 50 mM Tris-HCl pH 8.0, 500 mM NaCl, 20 mM imidazole supplemented with one EDTA-free protease inhibitor cocktail tablet (Roche) and DNAse (4 µg ml^{-1} final concentration). Cells in this resuspension were lysed by two passes through a One-Shot cell disruptor (Constant Systems) at 23 kpsi and the cell debris was removed by centrifugation (40,000 x g at 4°C for 30 min). The first purification step was affinity chromatography with a 5 mL HisTrap™ FF column (GE Healthcare) precharged with Ni^{2+} and equilibrated in buffer A (50 mM Tris-HCl, pH 8.0, 500 mM NaCl, 20 mM imidazole). A linear concentration gradient of imidazole was applied to elute the protein using buffer B (50

687 mM Tris-HCl, pH 8.0, 500 mM NaCl, 800 mM imidazole). Further purification was carried
688 out by size exclusion chromatography using a Superdex™ 200 Hi Load 16/60 column (GE
689 Healthcare). Proteins were eluted with SEC buffer (25 mM Tris-HCl, pH 8.0, 150mM NaCl)
690 and analysed by SDS-PAGE.
691
692 **Generation of anti-PBP1 antibody**
693 Serum against sPBP1A-BAP was produced from rabbits following a 28-day immunisation
694 program at Eurogentec (Belgium), and it was purified as previously described (Bertsche et
695 al., 2006).
696
697 **Immunoblot analysis**
698 *S. aureus* cultures were washed three times by resuspension and centrifugation (5,000 x g, 10
699 min, 4°C) in PBS. Cells were resuspended in TBSI (50 mM Tris, 100 mM NaCl, pH 8, plus
700 Complete Protease Inhibitor Cocktail, Roche) and broken using 0.1 mm silica spheres
701 (Lysing Matrix B) and FastPrep Homogenizer (MP Biomedicals) in 12 cycles of 30 s, at
702 maximum speed (6.5 m s^{-1}), with 5 min incubation on ice between cycles. Cell lysates were
703 centrifuged (5,000 x g, 10 min, 4°C) to remove unbroken cells. ~ 60 µg of total protein was
704 separated on a 12% (w/v) SDS-PAGE gel and electroblotted onto a nitrocellulose membrane
705 and blocked in 5% (w/v) skimmed-milk in TBST (20 mM Tris-HCl, pH 7.6; 17 mM NaCl,
706 0.1% (v/v) Tween-20). The membrane blocked in 5% (w/v) skimmed-milk in TBST (20 mM
707 Tris-HCl, pH 7.6; 17 mM NaCl, 0.1% (v/v) Tween-20) was incubated with primary
708 polyclonal anti-PBP1 (1:1,000) overnight with gentle agitation at 4°C. Primary antibodies
709 were detected using horseradish peroxidase-conjugated goat anti-rabbit IgG (1:10,000,
710 BioRad) and Clarity Western ECL Substrate (BioRad) reagent according to the

711 manufacturer's protocol. Chemiluminescence was detected using Syngene G:BOX Chemi
712 XX9.
713
714 **Crystallisation, data collection and structure determination**
715 Crystallisation of *Sa*PASTA$_{PBP1}$ was carried out at 20°C by the sitting-drop vapour diffusion
716 method in 96-well MRC plates (Molecular Dimensions) with a Mosquito crystallisation robot
717 (TTP LabTech) and commercial crystallisation screens (Hampton Research and Molecular
718 Dimensions). Orthorhombic crystals of diffraction quality, with a maximum dimension of
719 approximately 500 µm, appeared overnight from a mixture of equal volumes of protein
720 solution (42 mg ml^{-1} in 25 mM Tris-HCl, pH 8.0, 150 mM NaCl) and reservoir solution (0.2
721 M NaCl, 0.1 M sodium/potassium phosphate pH 6.2, 50 % (v/v) PEG 200). Diffraction data
722 were indexed and integrated using XDS (Kabsch, 2010) and scaled using AIMLESS (Evans
723 & Murshudov, 2013) from the CCP4 program suite (Winn et al., 2011). The crystals display
724 space group $P2_12_12_1$ with unit cell lengths a = 39.8 Å, b = 81.4 Å and c = 89.6 Å. The
725 asymmetric unit consists of two polypeptide chains with an estimated solvent content of 45 %
726 and a V_m of 2.24 Å^3/Da. The region corresponding to the two PASTA domains in the crystal
727 structure of *S. pneumoniae* PBP2x (PBP 5OAU) was used as a molecular replacement search
728 model, sharing approximately 26 % sequence identity with *Sa*PASTA$_{PBP1}$. The search model
729 was generated using phenix.sculptor (Bunkóczi & Read, 2011) to remove non-
730 macromolecular chains and prune sidechains. The structure was solved by molecular
731 replacement using PHASER (McCoy et al., 2007) and the resultant electron density map was
732 of high quality, allowing the tracing of the main chain. Model building and refinement were
733 carried out with Coot (Emsley et al., 2010) and Phenix (Liebschner et al., 2019), respectively.
734 Assessments of the geometry and validation of the final model was carried out using
735 Molprobity (Chen et al., 2010). Analyses of surface areas and interactions were made using

736 the PISA web service (Krissinel & Henrick, 2007). The graphics program PyMOL
737 (Schrödinger, LLC, 2015) was used to generate all molecular figures presented.
738
739 **Cell wall binding assays**
740 Cell wall binding assays of recombinant PBP1 proteins fluorescently labelled with Cy2 bis-
741 reactive dye (GE Healthcare) were performed as previously described (Bottomley et al.,
742 2014).
743
744 **Bacterial two-hybrid**
745 Competent BTH101 was co-transformed with pKT25 and pUT18 derivatives. Transformants
746 were selected on LB agar plates containing 100 μg ml^{-1} ampicillin, 50 μg ml^{-1} kanamycin
747 and 40 μg ml^{-1} X-Gal and incubated at 30°C. Single colonies were grown in 150 μl LB with
748 100 μg ml^{-1} ampicillin, 50 μg ml^{-1} kanamycin and 0.5 mM IPTG at 30°C.
749 To qualitatively measure for pairwise interactions, 5 μl of each overnight culture were spotted
750 onto LB agar plates containing 100 μg ml^{-1} ampicillin, 50 μg ml^{-1} kanamycin, 0.5 mM IPTG
751 and 40 μg ml^{-1} X-Gal. Plates were incubated at 30°C 24 – 48 h in an environment protected
752 from light and imaged. To quantify interactions, overnight cultures were assayed for β-
753 galactosidase activity against MUG (4-methylumbelliferyl-β-d-galactopyranoside) using an
754 assay as previously described (Steele et al., 2011).
755

756 ## Acknowledgements
757 This work was funded by the Medical Research Council (MR/N002679/1; MR/K015753/1),
758 UKRI Strategic Priorities Fund (EP/T002778/1) and the Wellcome Trust (212197/Z/19/Z).
759 L.L. thanks The Florey Institute for her PhD studentship. We gratefully acknowledge the
760 Wolfson Light Microscopy facility for their support and assistance in this work. We thank

761 Diamond Light Source for access to beamline I24 (mx18598) and Arnaud Baslé for data
762 collection, help with figure generation and support. We are grateful to Joshua Sutton, Grace
763 Pidwill, Victoria Lund, Laia Pasquina-Lemonche and Christopher Hill for help and advice.

764

765 ## Competing Interests

766 The authors declare no competing interests.

Figures and figure legends

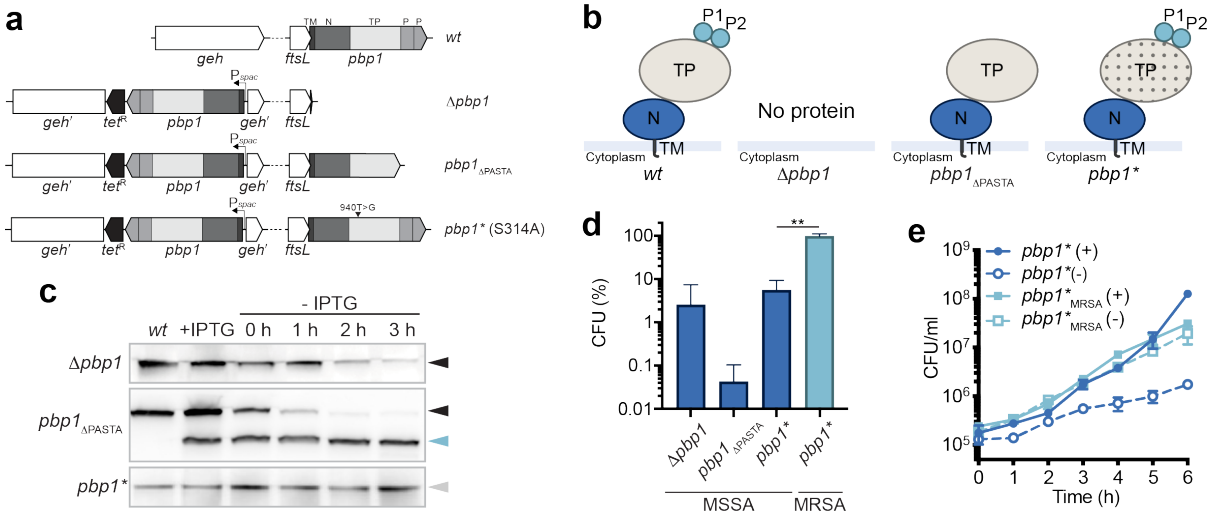

Fig. 1 Essentiality of PBP1

a, Schematic representation of genetic constructs used in this study. In *S. aureus* WT (*wt*) the 5′ end of *pbp1* overlaps with the 3′ of *ftsL*. The *pbp1* gene encodes a protein containing the transmembrane helix (TM), N-terminal domain (N), transpeptidase (TP) domain and two PASTA domains (P1 and P2). In the mutants, an ectopic copy of *pbp1* is placed under the control of the P*spac* promoter at the lipase (*geh*) locus, whereas the gene in the native *pbp1* locus is either deleted (Δ*pbp1*), has P1 and P2 domains removed ($pbp1_{\Delta PASTA}$), or has a point mutation which results in inactivation of the TP domain (*pbp1**).

b, Schematic representation of domain architecture of PBP1 in *S. aureus* WT (*wt*) and PBP1 forms produced by Δ*pbp1*, $pbp1_{\Delta PASTA}$ and *pbp1** mutants in the absence of inducer. The TP domain inactivation is shown by dotted shading.

c, Immunoblot showing PBP1 levels in SH1000 *lacI* (*wt*) and in Δ*pbp1*, $pbp1_{\Delta PASTA}$ and *pbp1** grown with IPTG (+IPTG) and for 0, 1, 2 and 3 h without inducer (-IPTG) analysed using anti-PBP1 antibody. Expected sizes: PBP1 and PBP1* = 83 kDa (black and grey arrowheads, respectively) and $PBP1_{\Delta PASTA}$ = 67 kDa (light blue arrowhead).

785 **d**, Plating efficiency of Δ*pbp1*, *pbp1*$_{\Delta PASTA}$ and *pbp1** (MSSA) cells and MRSA *pbp1**

786 (*pbp1**$_{MRSA}$) cells upon inducer removal compared to the control groups grow in the presence

787 of inducer. *P* value was determined by Mann–Whitney *U* tests. $P = 0.0043$ (**, $P < 0.01$).

788 Data represent mean ± SD.

789 **e**, Growth curves of *pbp1** (MSSA) and MRSA *pbp1**(*pbp1**$_{MRSA}$) in the presence (+) or

790 absence (-) of IPTG. Data represent mean ± SD. Error bars that are smaller than the symbols

791 are not shown.

792

793 Data are representative of three (c, e) and at least four (d) independent experiments.

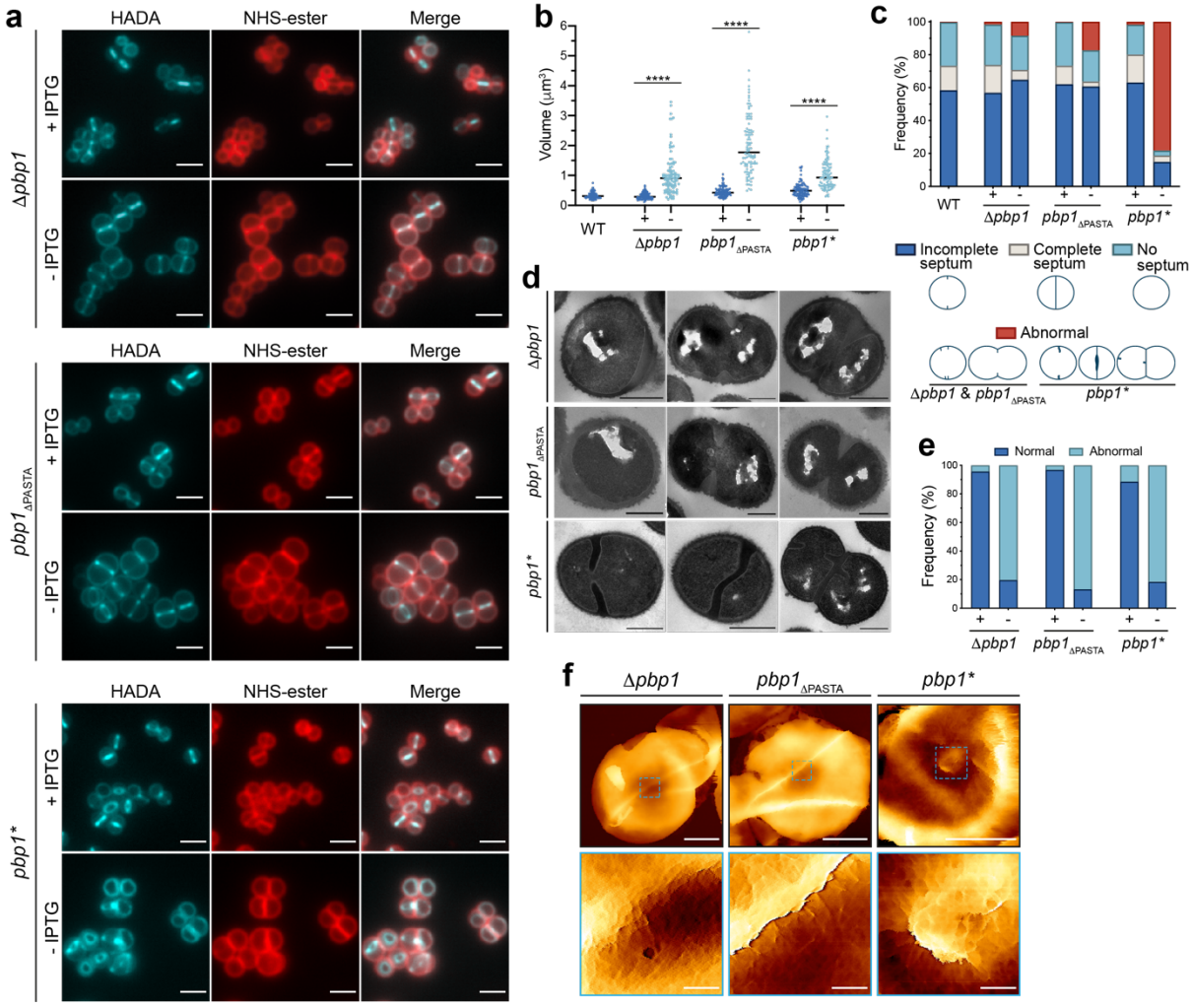

794

795 **Fig. 2 The role of PBP1 in cell division and PG synthesis in *S. aureus*.**

796 **a**, Δ*pbp1*, *pbp1*$_{\Delta PASTA}$ and *pbp1** grown with or without IPTG for 2 h, incubated with HADA
797 for 5 min to show nascent PG, and counter-labelled with NHS-ester Alexa Fluor 555 to
798 image the cell wall. Images are average intensity projections of *z* stacks. Scale bars 2 μm.
799 **b**, Cell volumes of WT (*wt*), Δ*pbp1*, *pbp1*$_{\Delta PASTA}$ and *pbp1** grown with (+) or without (-)
800 IPTG for 2 h as measured by fluorescence microscopy after NHS-ester Alexa Fluor 555
801 labelling. Each dot represents a single cell. The median of each distribution is indicated by a
802 black line. The number of cells analysed for each mutant and condition was $n \geq 100$. *P* value
803 was determined by Mann–Whitney *U* tests (****, $P < 0.0001$). From left to right: $P = 3.033e\text{-}033$, 4.670e-049 and 2.206e-022; $n = 100, 101, 100, 101, 100, 100$ and 101.

c, Quantification of cellular phenotypes for WT *(wt), Δpbp1, pbp1*$_{\Delta PASTA}$ and *pbp1** based on HADA incorporation (Fig. 2a) after incubation with (+) or without (-) IPTG for 2 h. From left to right n = 370, 427, 332, 314, 364, 512 and 331.

d, TEM of Δ*pbp1, pbp1*$_{\Delta PASTA}$ and *pbp1** grown for 2 h in the absence of inducer. Scale bars 500 nm.

e, Quantification of cellular phenotypes based on TEM data of Δ*pbp1, pbp1*$_{\Delta PASTA}$ and *pbp1** grown for 2 h in the presence (+) or absence (-) of IPTG. Examples of cells classified as normal (blue) are shown in Fig. 2 – figure supplement 2b. Cells with abnormal phenotypes (light blue) are shown in Fig. 2d and Fig. 2 – figure supplement 2c. From left to right n = 391, 329, 314, 377, 263 and 302.

f, AFM topographic images of internal surface of purified sacculi from Δ*pbp1, pbp1*$_{\Delta PASTA}$ and *pbp1** grown in the absence of inducer for 2 h. Sacculi (top images, scale bars 500 nm, data scales (z): 450, 300 and 100 nm from left to right, respectively) and higher magnification images (bottom images, scale bars 50 nm, data scales (z): 70, 100 and 50 nm from left to right respectively) scanned within the boxed areas from the top images.

Data are representative of two (d-f) and (a-c) three independent experiments.

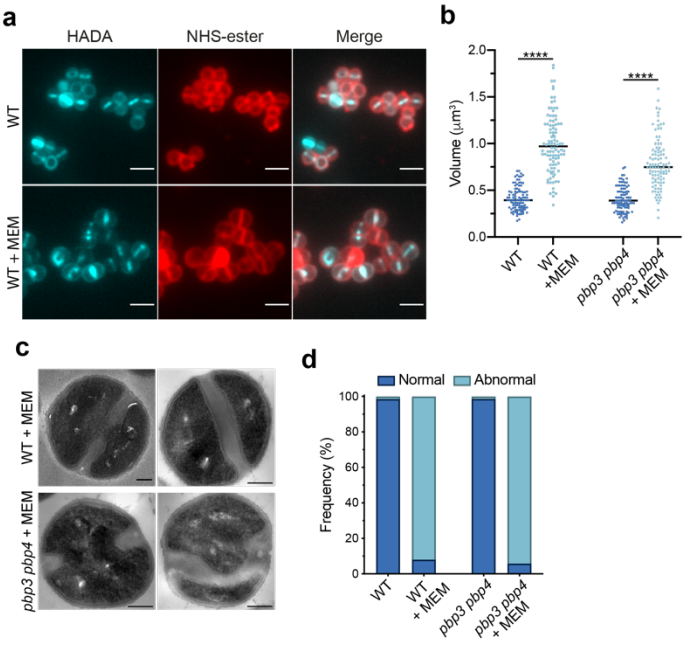

Fig. 3 Effect of meropenem (MEM), an antibiotic with high affinity for PBP1, on *S. aureus*.

a, Fluorescence images of SH1000 WT treated with 1x MIC MEM for 1 h, labelled with HADA for 5 min to show nascent PG and counter labelled with NHS-ester Alexa Fluor 555 (cell wall). Images are average intensity projections of *z* stacks. Scale bars 2 μm.

b, Cell volumes of SH1000 WT and *pbp3 pbp4* treated with 1x MIC MEM for 1 h as measured by fluorescence microscopy after NHS-ester Alexa Fluor 555 labelling (Fig. 3a). Each dot represents a single cell. The median of each distribution is indicated by a black line. The number of cells analysed for each condition was $n \geq 100$. *P* value was determined by Mann–Whitney *U* tests (****, $P < 0.0001$). From left to right: $P = 1.276e\text{-}042$ and 1.421e-024; $n = 102$, 100, 101 and 102.

c, TEM of SH1000 WT and *pbp3 pbp4* treated with 1x MIC MEM for 1 h. Scale bars 200 nm.

d, Quantification of phenotypes of SH1000 WT and *pbp3 pbp4* treated with MEM (1x MIC) for 1 h based on TEM data (Fig. 3c and Fig. 3 – figure supplement 1e, f). Examples of cells classified as normal (blue) are shown in Fig. 3 – figure supplement 1e, f. Cells with abnormal

839 phenotypes (light blue) are shown in Fig. 3c and Fig. 3 – figure supplement 1e, f. From left to

840 right *n*= 343, 287, 275 and 172.

841

842 Data are representative of two (a, b (for WT) independent experiments. Experiments in b (for

843 *pbp3 pbp4)* and d were performed once.

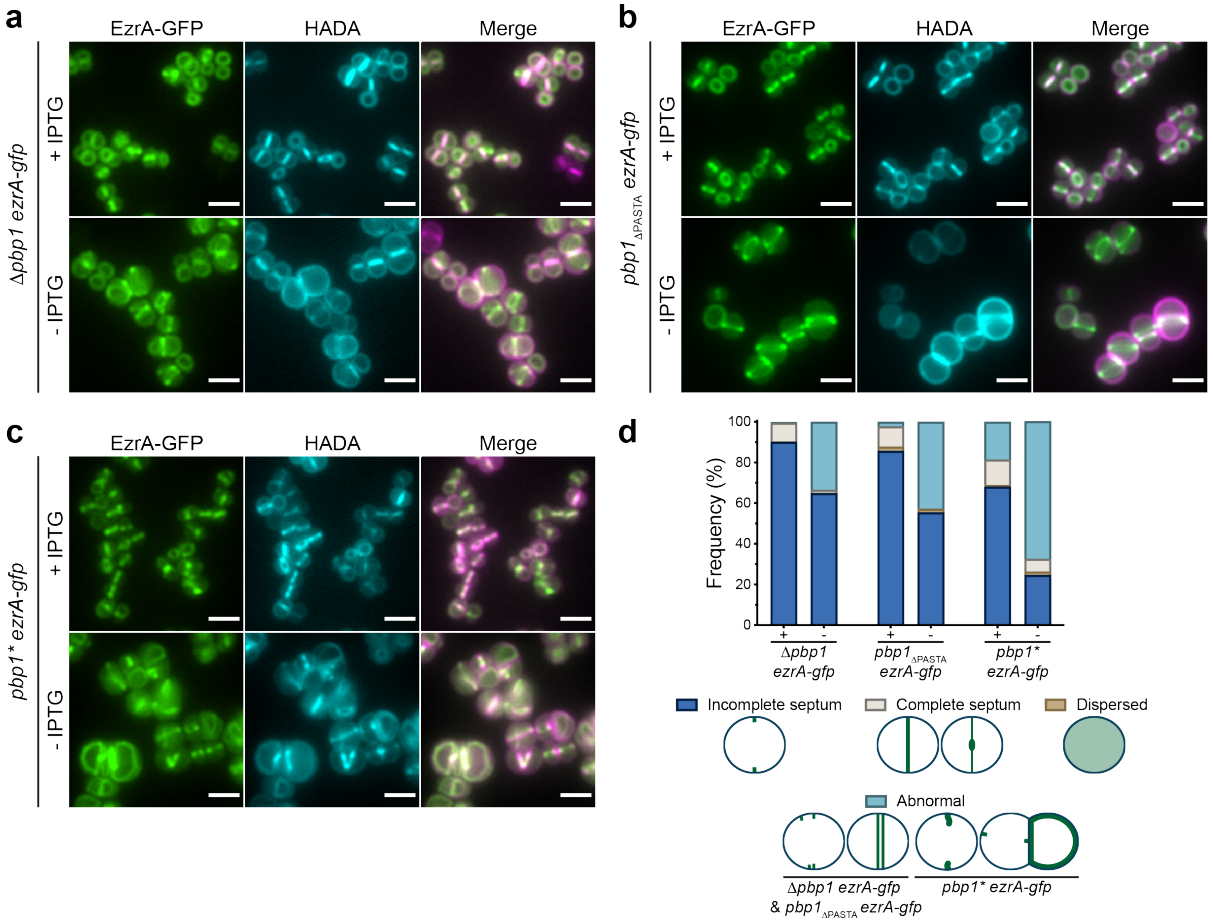

Fig. 4 The role of PBP1, PASTA and TP domains in EzrA localisation in *S. aureus*.

a-c, Localisation of EzrA-GFP in Δ*pbp1 ezrA-gfp, pbp1*$_{\Delta PASTA}$ *ezrA-gfp* and *pbp1* ezrA-gfp* grown in the presence or absence of IPTG for 2 h and labelled with HADA for 5 min to stain PG. Images are average intensity projections of *z* stacks. Scale bars 5 µm.

d, Quantification of EzrA-GFP localisations in Δ*pbp1 ezrA-gfp*, *pbp1*$_{\Delta PASTA}$ *ezrA-gfp* and *pbp1* ezrA-gfp* grown with or without IPTG. From left to right n = 395, 499, 481, 438, 360 and 382.

Data are representative of two independent experiments.

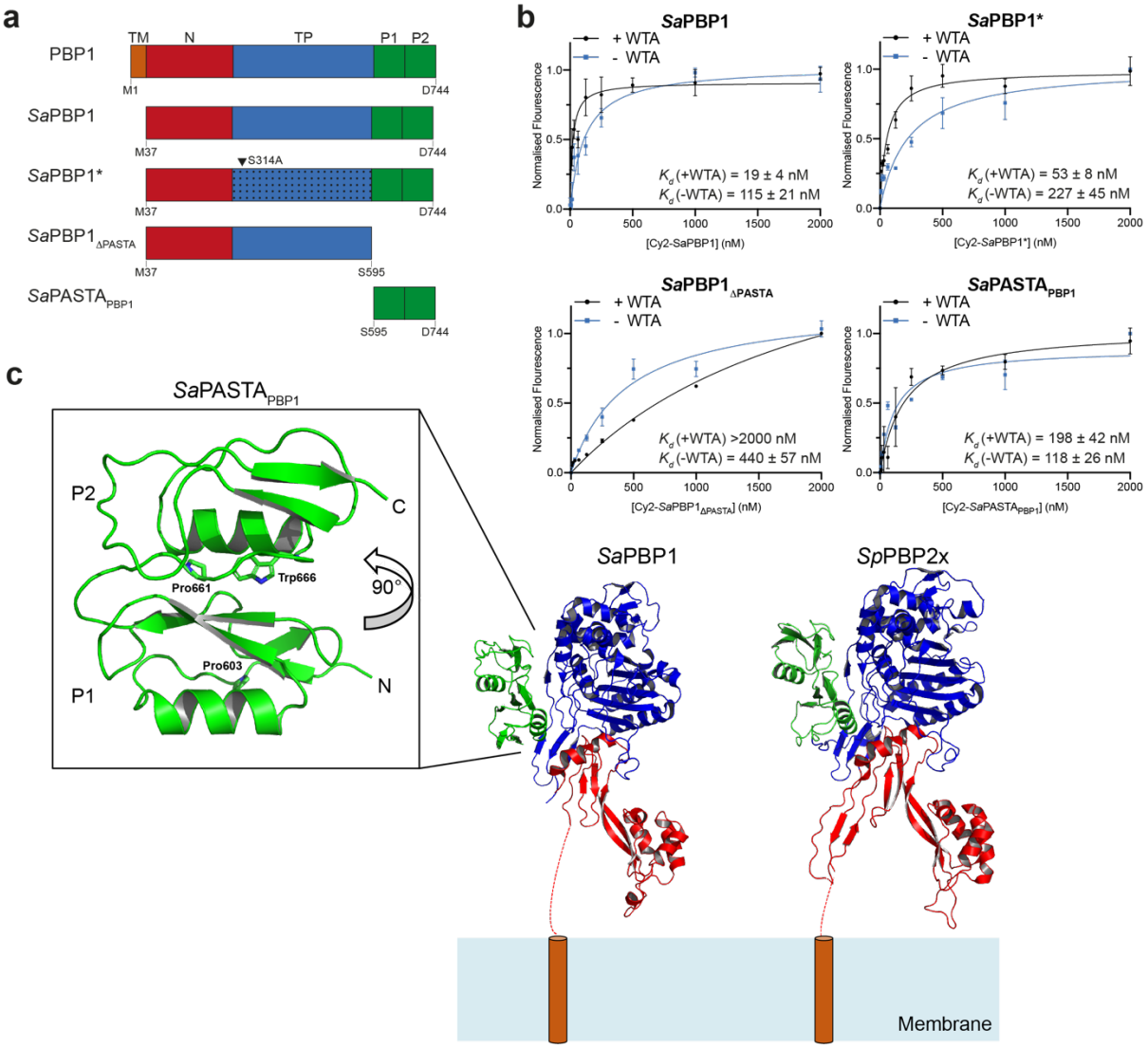

Fig. 5 Role of PBP1 PASTA domains in cell wall binding

a, Schematic representation of structural domain organization of *S. aureus* PBP1 (top) and recombinant proteins (*Sa*PBP1, *Sa*PBP1$_{\Delta PASTA}$, *Sa*PBP1* and *Sa*PASTA$_{PBP1}$) used in this study. TM, trans-membrane helix (orange); N, N-terminal dimerization domain (red); TP, transpeptidase domain (blue); P, PASTA domains (green). The arrowhead indicates the inactivation substitution in the TP domain of *Sa*PBP1*. The first and last amino acids of constructs are indicated.

b, Fluorescent cell wall sedimentation assay. A Wilcoxon signed rank test ($P < 0.05$) was carried out to assess the significance of difference in +WTA/-WTA PG binding: *Sa*PBP1, $P = 0.0273$; *Sa*PBP1*, $P = 0.0078$; *Sa*PBP1$_{\Delta PASTA}$, $P = 0.0195$; *Sa*PASTA$_{PBP1}$, $P \geq 0.9999$,

not significant. Data represent mean ± SD. Error bars that are smaller than the symbols are not shown.

c, Structure of *Sa*PASTA$_{PBP1}$. The crystal structure of *S. aureus* PBP1 lacking the PASTA domains (*Sa*PBP1, PDB 5TRO) and our *Sa*PASTA$_{PBP1}$ structure were superimposed on to *S. pneumoniae* PBP2x (*Sp*PBP2x, PDB 5OAU) and displayed as cartoons. Their N-termini are orientated close to the representative cell membrane, as if anchored there by their respective transmembrane helices (dashed red line/orange cylinder). Individual domains are coloured as follows; N-terminal domain (red), transpeptidase domain (blue) and PASTA domain (green). The individual PASTA domains are labelled P1 and P2, respectively. Residues Pro603, Pro661 and Trp666 are displayed as sticks, with nitrogen atoms coloured blue.

Supplementary figures and legends

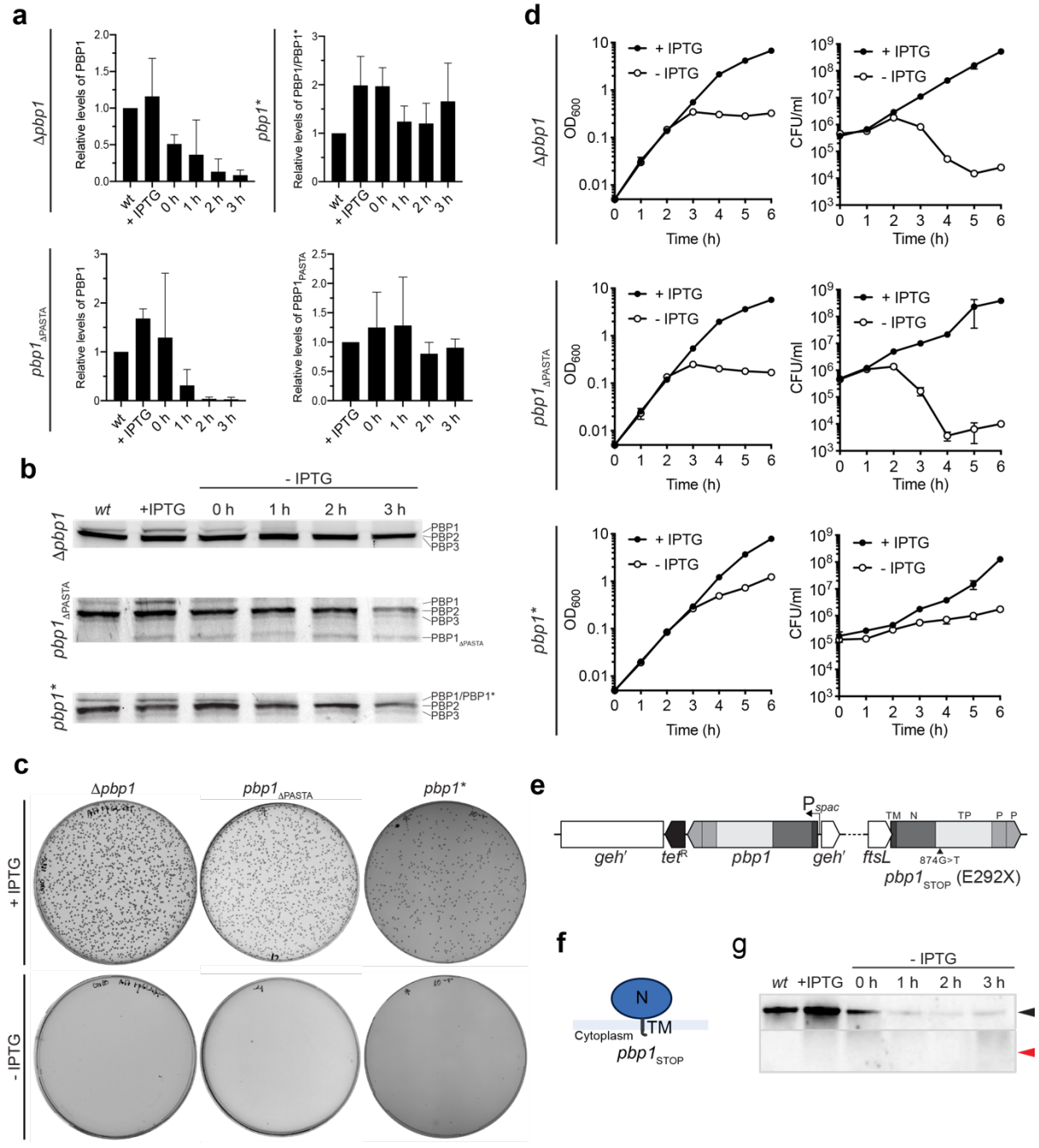

Fig. 1 – figure supplement 1. Essentiality of PBP1, PASTA and TP domains in *S. aureus.*

a, Relative levels of PBP1 in Δ*pbp1, pbp1*$_{\Delta PASTA}$ and *pbp1** grown with IPTG and for 0, 1, 2 and 3 h after inducer removal. PBP1 levels were normalized to protein levels in SH1000 *lacI*

882 (*wt*). PBP1$_{\Delta PASTA}$ levels were normalized to PBP1$_{\Delta PASTA}$ levels in the presence of inducer.
883 Quantifications are for the data shown in Fig. 1c. Data represent mean ± SD.
884 **b**, BocillinFL gel-based analysis of penicillin binding proteins in SH1000 *lacI* (*wt*) and
885 Δ*pbp1, pbp1*$_{\Delta PASTA}$ and *pbp1** grown with IPTG and 0, 1, 2 and 3 h after inducer removal.
886 **c**, Growth of Δ*pbp1, pbp1*$_{\Delta PASTA}$ and *pbp1** with or without IPTG. Quantifications for the
887 plate assay are shown in Fig. 1d.
888 **d**, Growth curves of Δ*pbp1, pbp1*$_{\Delta PASTA}$ and *pbp1** in the presence or absence of IPTG. Data
889 represent mean ± SD. Error bars that are smaller than the data point symbols are not shown.
890 **e**, Schematic representation of the *pbp1*$_{STOP}$ mutant. A SNP (874 G for T) resulted in a
891 premature stop codon (E292X) and removal of the TP and PASTA domains.
892 **f**, Schematic representation of domain architecture of PBP1$_{STOP}$ encoded by the *pbp1*$_{STOP}$
893 mutant.
894 **g**, Immunoblot showing PBP1 levels in SH1000 *lacI* (*wt*) and *pbp1*$_{STOP}$ grown with IPTG and
895 for 0, 1, 2 and 3 h without inducer analysed using anti-PBP1 antibody. Expected sizes: PBP1
896 = 83 kDa (black arrowhead) and PBP1$_{STOP}$ = 33 kDa (red arrowhead).
897
898 Data are representative of two (g), three (a, b, d) and at least four (c) independent
899 experiments.

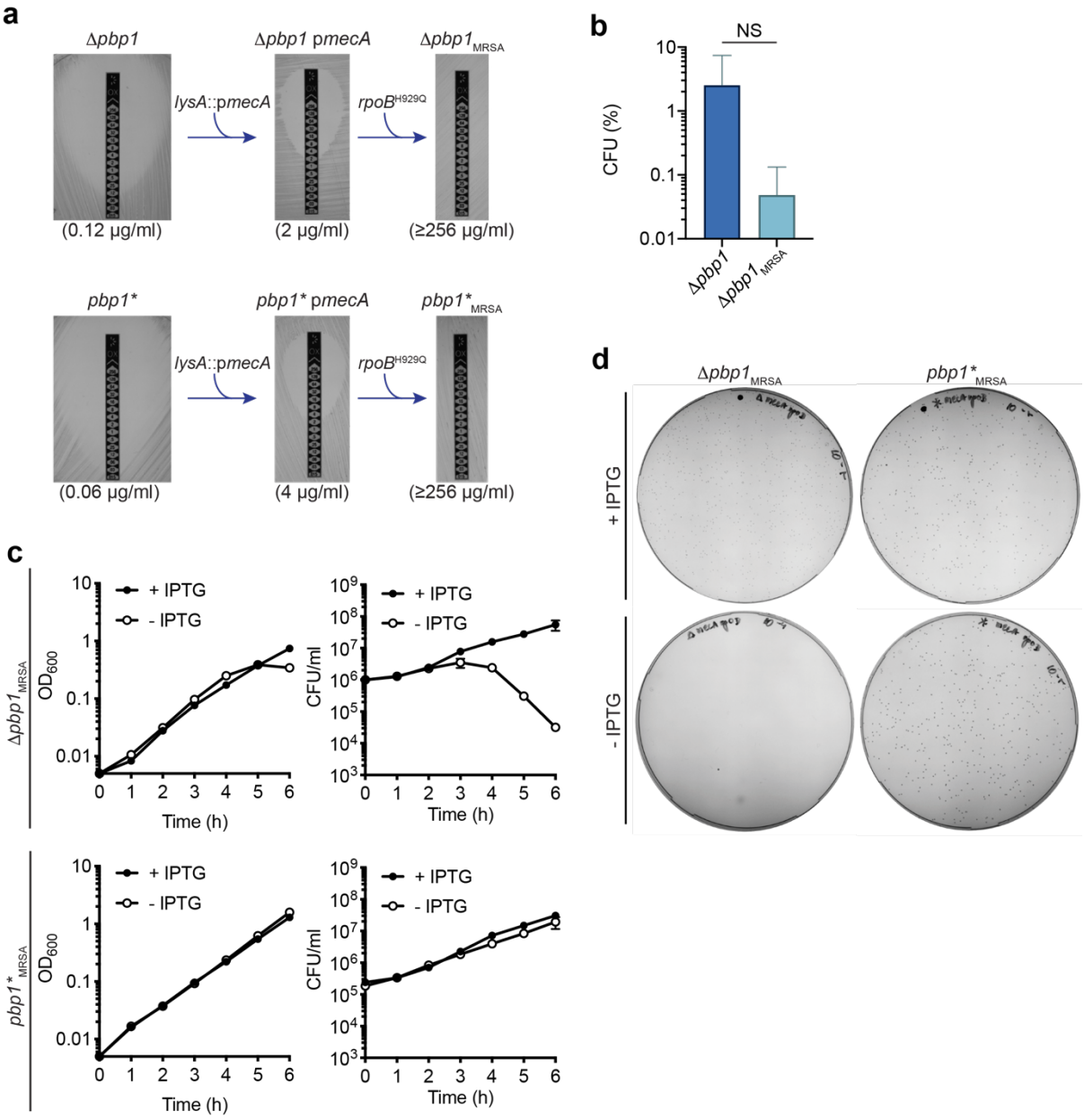

Fig. 1 – figure supplement 2. Essentiality of PBP1 and its TP activity in Methicillin-resistant *S. aureus*.

a, Schematic representation of evolution of high-level β-lactam resistant Δ*pbp1* and *pbp1**. A single copy *mecA* under its native promoter (p*mecA*) was introduced at the *lysA* locus, resulting in low-level oxacillin resistant Δ*pbp1* p*mecA* and *pbp1** p*mecA*. Subsequently, addition of a point mutation in the *rpoB* gene results in development of high-level resistant Δ*pbp1*$_{MRSA}$ and *pbp1**. Oxacillin MICs shown in brackets were measured using the E-test strips.

b, Plating efficiency of Δ*pbp* (MSSA) and MRSA Δ*pbp1*$_{MRSA}$ cells upon the inducer removal compared to the control groups grown in the presence of inducer. Data represent mean ± SD. *P* value was determined by Mann–Whitney *U* tests. $P = 0.5429$ (NS, not significant).

c, Growth curves of Δ*pbp1*$_{MRSA}$ and *pbp1**$_{MRSA}$ in the presence or absence of IPTG. Data represent mean ± SD. Error bars that are smaller than the data point symbols are not shown.

d, Growth of Δ*pbp1*$_{MRSA}$ and *pbp1**$_{MRSA}$ with or without IPTG. Quantifications for Δ*pbp1*$_{MRSA}$ are shown in Fig. 1 – figure supplement 2c and for *pbp1**$_{MRSA}$ are shown in Fig. 1b.

Data are representative of at least three independent experiments.

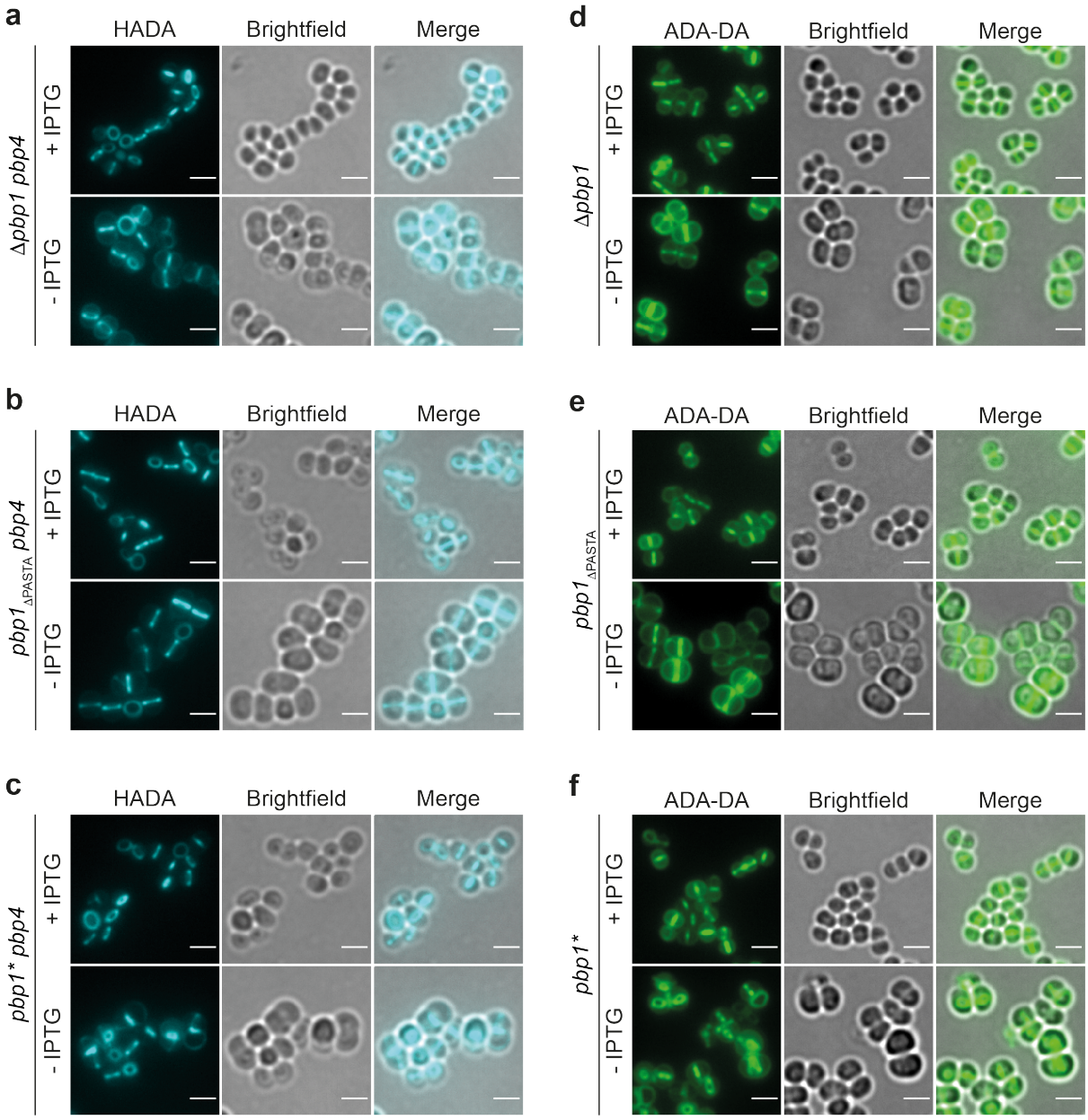

Fig. 2 – figure supplement 1. Loss of PBP1, PASTAs or TP activity of PBP1 does not prevent PG synthesis.

a-c, PG incorporation in *pbp4* mutants depleted of PBP1. Δ*pbp1 pbp4, pbp1*$_{\Delta PASTA}$ *pbp4* and *pbp1* pbp4* grown with or without IPTG for 2 h and incubated with HADA for 5 min to show nascent PG incorporation.

d-f, Δ*pbp1, pbp1*$_{\Delta PASTA}$ and *pbp1** grown with or without IPTG for 2 h, incubated with dipeptide (ADA-DA) for 5 min and clicked to Alexa Fluor 488 to show nascent PG incorporation.

928 Fluorescence images are average intensity projections of *z* stacks. Scale bars 2 μm.

929

930 Images are representatives of two independent experiments.

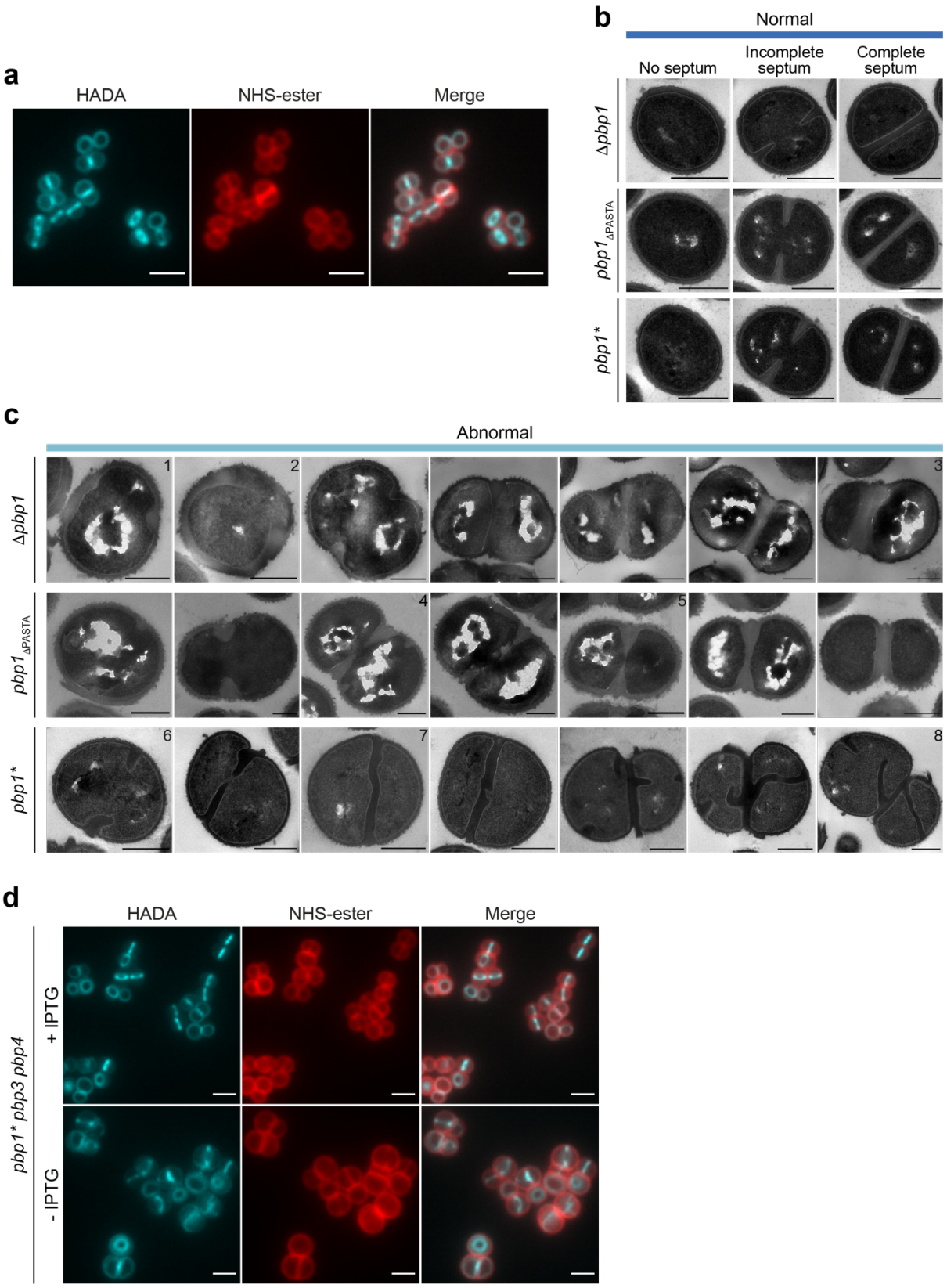

931

932 **Fig. 2 – figure supplement 2. Role of PBP1 in *S. aureus***

933 **a**, Fluorescence images of SH1000 WT labelled with HADA for 5 min (nascent PG) and
934 counter labelled with NHS-ester Alexa Fluor 555 (cell wall). Images are average intensity
935 projections of *z* stacks. Scale bars 2 μm.
936 **b**, TEM of Δ*pbp1, pbp1*$_{\Delta PASTA}$ and *pbp1** grown in the presence of IPTG categorised as
937 normal phenotype (blue). Scale bars 500 nm.
938 **c**, TEM of Δ*pbp1, pbp1*$_{\Delta PASTA}$ and *pbp1** grown in the absence of IPTG for 2 h categorised
939 as abnormal phenotype (1, PG blebs; 2, thickened cell wall; 3, thickened complete septum; 4,
940 multiple septa; 5, misshapen incomplete septum; 6, thick incomplete septum with rounded
941 leading edge; 7, curved septum; 8, separation defect. Scale bars 500 nm.
942 **d**, Fluorescence images of *pbp1* pbp3 pbp4* grown with or without IPTG for 2 h, labelled
943 with HADA for 5 min (nascent PG) and counter stained with NHS-ester Alexa Fluor 555
944 (cell wall). Images are average intensity projections of *z* stacks. Scale bars 2 μm.
945
946 Data are representative of two independent experiments.

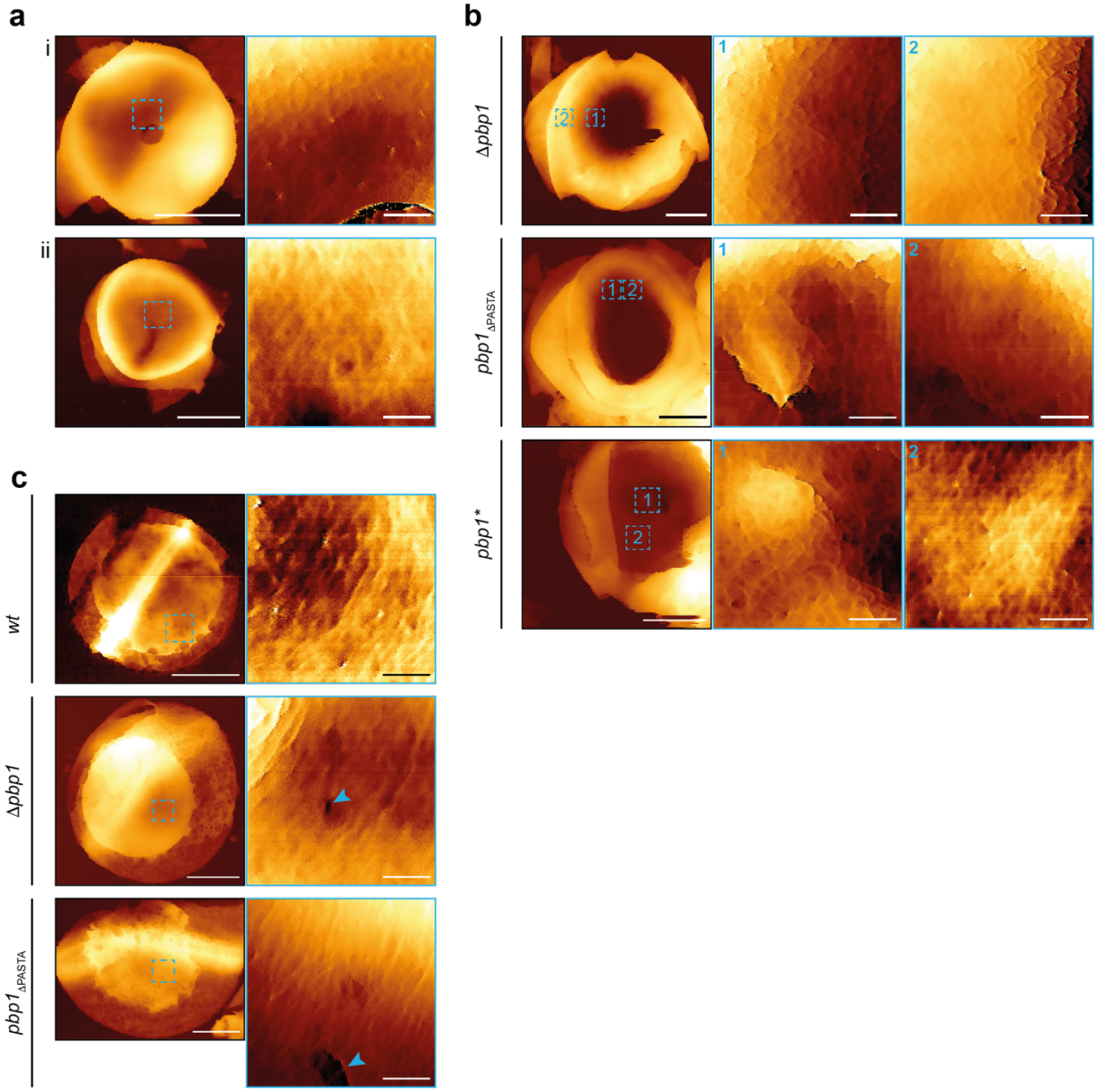

Fig. 2 – figure supplement 3. Gallery of AFM images of *S. aureus* Δ*pbp1*, *pbp1*$_{\Delta PASTA}$ and *pbp1

a, AFM topographic images of unfinished (i) and closed (ii) septa in *S. aureus* SH1000. Sacculi (images to the left, scale bars 500 nm, data scales (*z*): 200 (top) and 250 nm (bottom)) and higher magnification scans (images to the right, scale bars 50 nm, data scales (*z*): 80 (top) and 40 nm (bottom)) on the boxed areas from the images to the left.

b, AFM topographic images of unfinished septa in Δ*pbp1* (from left to right: scale bars 500, 50 and 50 nm; data scales (*z*) 500, 120 and 150 nm), *pbp1*$_{\Delta PASTA}$ (from left to right: scale bars 500, 50 and 50 nm; data scales (*z*) 693, 80 and 100 nm) and *pbp1** (from left to right: scale

957 bars 500, 50 and 50 nm; data scales (*z*) 500, 80 and 25 nm) grown in the absence of inducer
958 for 2 h. Images to the left are sacculi, while images in the centre (1) and to the right (2) are
959 higher magnification scans on the boxed areas of the images on the left.
960 **c**, AFM topographic images of external nascent ring architecture in SH1000 WT (*wt*; scale
961 bars: from left to right: scale bars 500 and 50 nm; data scales (*z*) 100 and 20 nm) and mutants
962 Δ*pbp1* (scale bars: from left to right: scale bars 500 and 50 nm; data scales (*z*) 400 and 60
963 nm) and *pbp1*$_{\Delta PASTA}$ (scale bars: from left to right: scale bars 500 and 50 nm; data scales (*z*)
964 350 and 100 nm) grown in the absence of inducer for 2 h. Images to the left are sacculi, while
965 images to the right are higher magnification scans on the boxed areas of the images on the
966 left. The arrowheads indicate abnormal features, holes.
967
968 Data are representative of two independent experiments.

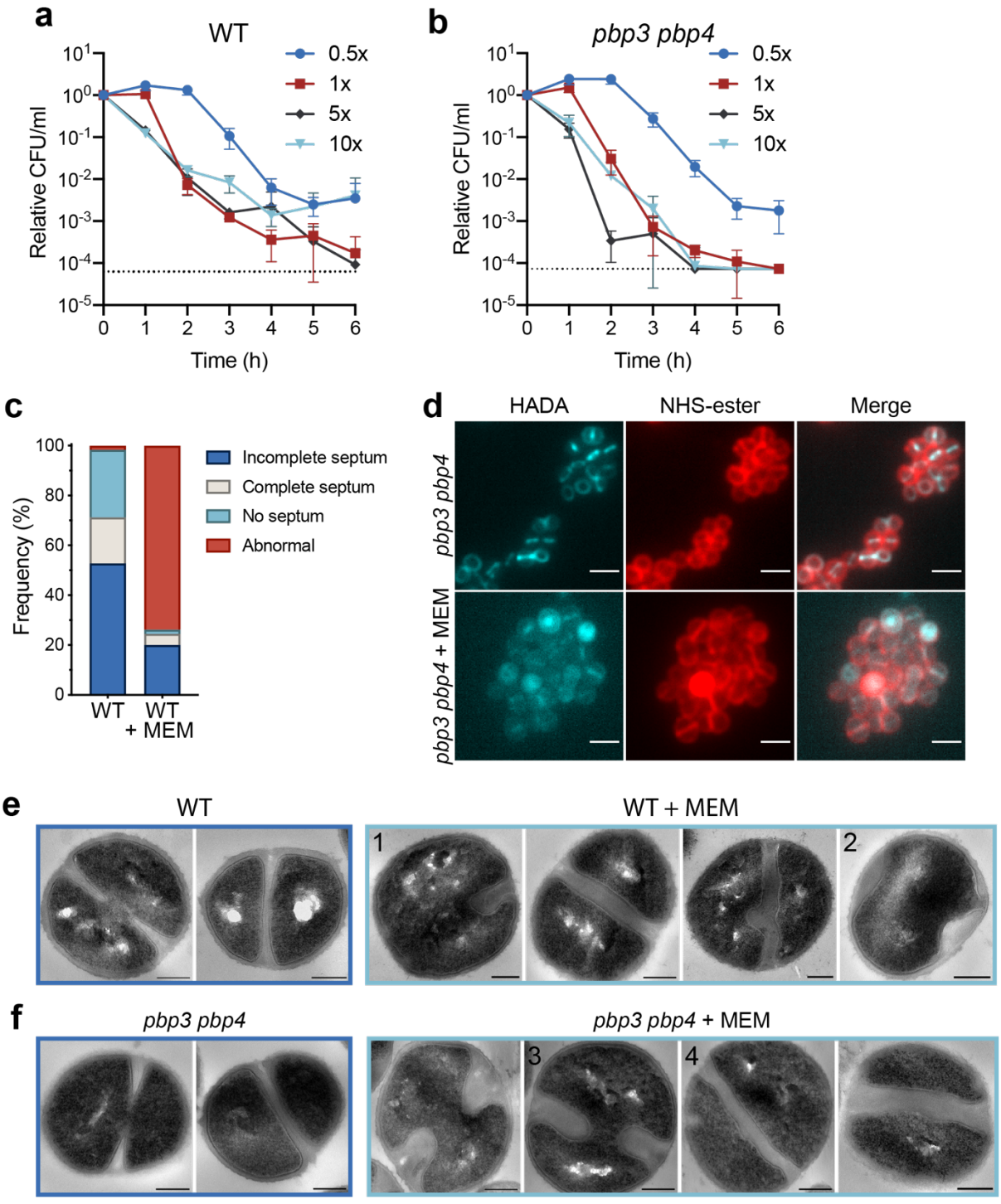

Fig. 3 – figure supplement 1. Effect of meropenem (MEM) on *S. aureus.*

a-b, Bactericidal effect of addition of 0.5x, 1x, 5x and 10x MIC MEM on (a) SH1000 WT and (b) *pbp3 pbp4* (b). MEM MIC is 0.4 µg/ml and 0.2 µg/ml for SH1000 WT and *pbp3 pbp4*, respectively Data represent mean ± SD. Error bars that are symbols than the dots are not shown. The dotted line is the detection limit.

c, Quantification of cellular phenotypes of SH1000 WT treated with 1x MIC MEM for 1 h based on HADA incorporation (Fig 3a). Same phenotype classification was used as shown in Fig. 2c. From left to right n = 309 and 355.

d, Fluorescence images of *pbp3 pbp4* treated with 1x MIC MEM for 1 h, labelled with HADA for 5 min to show nascent PG and counter labelled with NHS-ester Alexa Fluor 555 (cell wall). Images are average intensity projections of z stacks. Scale bars 2 μm. Phenotype classification of MEM treated *pbp3 pbp4* was not possible due to low HADA fluorescence signal.

e-f, TEM of SH1000 WT (e) and *pbp3 pbp4* (f) grown with or without 1x MIC MEM for 1 h. Scale bars 200 nm. Examples of cells categorised as normal phenotype are in blue, cells with abnormal phenotype are in light blue (1, asymmetric septum ingrowth; 2, off-septal PG thickening; 3, septum with rounded leading edge; 4, curved septum).

Data are representative of three (a and b) and two (c) independent experiments. Experiments in d, e and f were performed once.

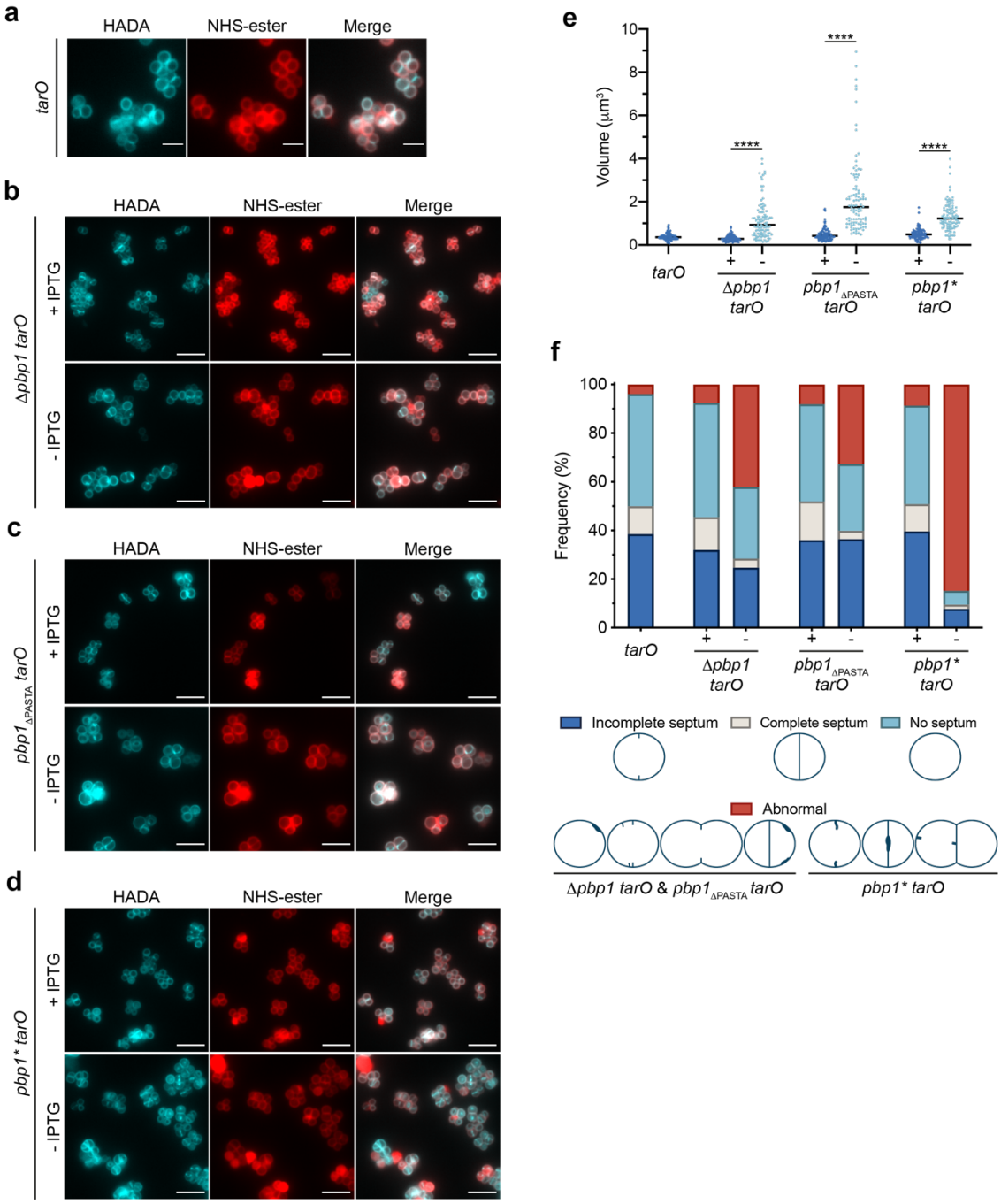

990

991 **Fig. 4 – figure supplement 1. Functional association between PBP1 and WTA**

992 **a**, Fluorescence images of the *tarO* mutant labelled with HADA for 5 min (nascent PG) and

993 counter stained with NHS-ester Alexa Fluor 555 (cell wall). Images are average intensity

994 projections of *z* stacks. Scale bars 5 μm.

995 **b-d**, Δ*pbp1 tarO, pbp1*$_{\Delta PASTA}$ *tarO* and *pbp1* tarO* grown with or without IPTG for 2 h,

996 incubated with HADA for 5 min to show nascent PG and counter labelled with NHS-ester

997 Alexa Fluor 555 (cell wall). Images are average intensity projections of *z* stacks. Scale bars 5
998 µm.
999 **e**, Cell volumes of *tarO* and Δ*pbp1 tarO, pbp1*$_{\Delta PASTA}$ *tarO* and *pbp1* tarO* grown with or
1000 without IPTG as measured by fluorescence microscopy after NHS-ester Alexa Fluor 555
1001 labelling. Each dot represents a single cell. The median of each distribution is indicated by a
1002 black line. The number of cells analysed for each mutant and condition was $n \geq 100$. *P* value
1003 was determined by Mann–Whitney *U* tests (***, $P < 0.0001$). From left to right: $P = 2.243e-$
1004 022, 1.460e-037 and 8.074e-029; $n = 100, 102, 101, 100, 100, 100$ and 100.
1005 **f**, Quantification of cellular phenotypes for *tarO* and Δ*pbp1 tarO, pbp1*$_{\Delta PASTA}$ *tarO* and
1006 *pbp1* tarO* based on HADA incorporation (Fig. 4 – figure supplement 1a-d) after incubation
1007 with or without IPTG. From left to right $n = 306, 253, 271, 358, 266, 313$ and 336.
1008
1009 Data are representative of two independent experiments.

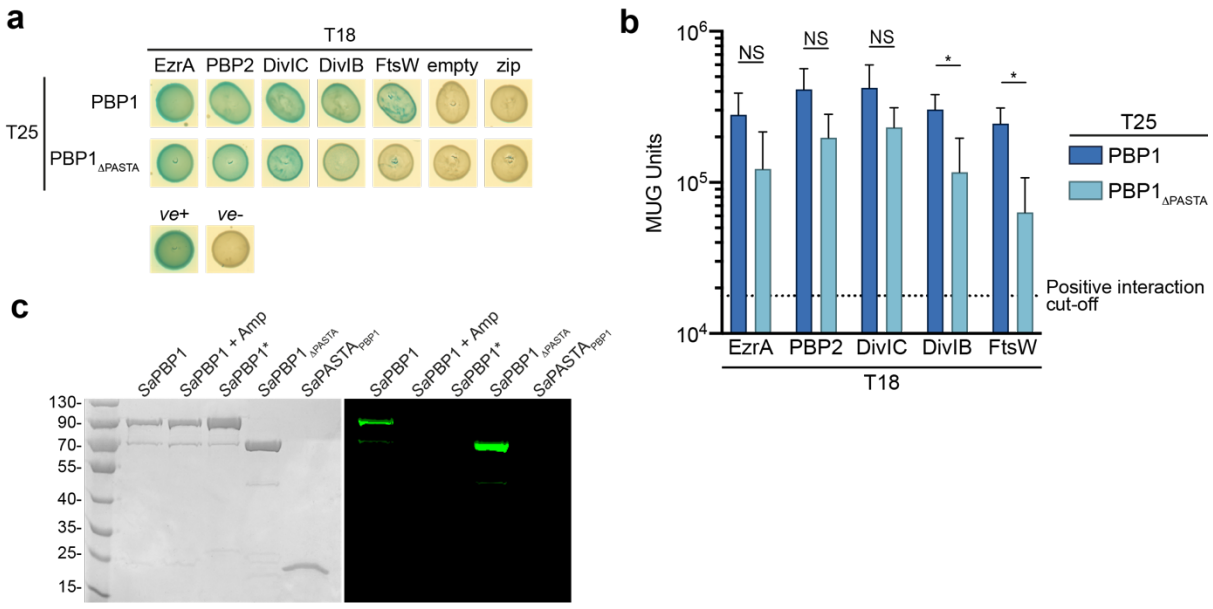

Fig. 5 – figure supplement 1. The role of PBP1 PASTA domains in interactions with cell division components and PG.

a, Bacterial two-hybrid analysis of the effect of PASTA domains truncation on PBP1 interaction with its known interaction partners; empty, T18 with no insert; zip, T18 with a leucine zipper fragment; *ve*+, positive control (T18-zip/T25-zip); *ve*-, negative control (T18/T25).

b, Quantitative bacterial two-hybrid analysis of the effect of the PASTA domains truncation on PBP1 interaction with cell division components determined by analysis of the β-galactosidase activities of *E. coli* BTH101 cells harbouring the corresponding plasmids. Dotted line, the positive interaction cut off value (4-fold greater than the pair of T18/T25). Data represent mean ± SD. *P* value was determined by Mann–Whitney *U* tests (*, $P < 0.05$). DivIB (PBP1 *vs* PBP1$_{\Delta PASTA}$) $P = 0.0424$, FtsW (PBP1 *vs* PBP1$_{\Delta PASTA}$) $P = 0.0163$.

c, Coomassie-stained SDS-PAGE gel (left) and BocillinFL gel-based analysis (right) of purified recombinant *Sa*PBP1, *Sa*BPP1*, *Sa*PBP1$_{\Delta PASTA}$ and *Sa*PASTA$_{PBP1}$. Bands corresponding to *Sa*PBP1 and *Sa*PBP1$_{\Delta PASTA}$ were fluorescent, indicating their covalent binding to BocillinFL. Bands corresponding to *Sa*PBP1* and *Sa*PASTA$_{PBP1}$ were not fluorescent, and were therefore unable to bind BocillinFL. *Sa*PBP1 incubated with ampicillin

1028 prior to BocillinFL incubation failed to fluoresce, consistent with specific binding of

1029 BocillinFL to the TP domain. Expected sizes: *Sa*PBP1 and *Sa*PBP1*, 80.5kDa;

1030 *Sa*PBP1$_{\Delta PASTA}$, 64.5 kDa; *Sa*PASTA$_{PBP1}$, 18.2 kDa.

1031

1032 Data are representative of two (c) and three (a-b) independent experiments.

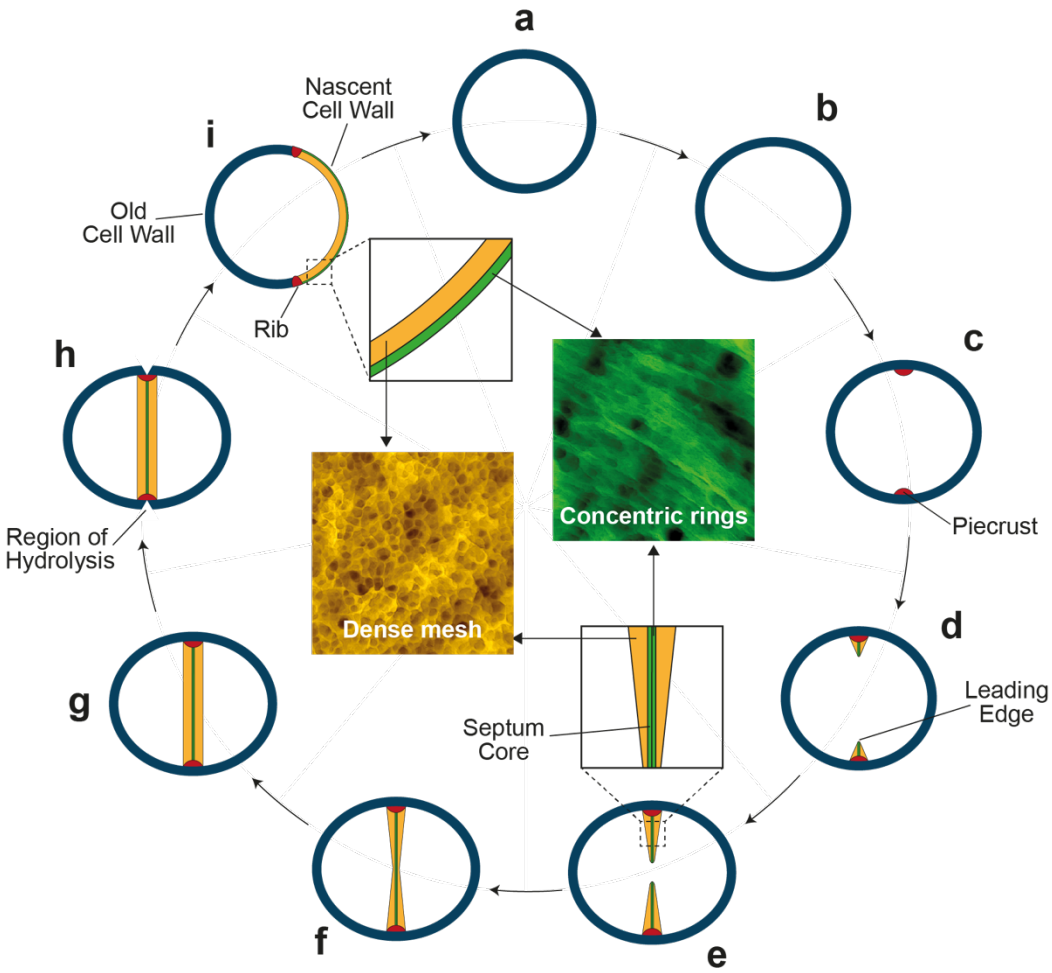

Fig. 5 – figure supplement 2. Conceptual model of septum formation in *S. aureus*.

(a, b) The growing *S. aureus* cell increases in volume (Zhou et al., 2015). (c) Septal synthesis starts by formation of the piecrust (red) (Turner et al., 2010). (d. e) 'V' shaped septum (Lund et al., 2018) progresses inwards by insertion of ring like structured PG synthesised by PBP1-FtsW at the septum core and mesh structured PG produced by PBP2. (f) The annulus closes resulting in a bowed septum. (g) Septum is filled out by peptidoglycan insertion executed by PBP2 and this continues until the cross wall is of uniform thickness (Lund et al., 2018). (h) Cell wall is hydrolysed at the plane of septation. (i) Daughter cells separate. The cell wall of the daughter cell (coloured insets) is a chimera of the old cell wall with both internally and externally mesh structured PG and a nascent cell wall with the external ring structured PG and the mesh-like cytoplasmic facing PG (Pasquina-Lemonche et al., 2020).

References

Arnaud, M., Chastanet, A., & Débarbouillé, M. (2004). New vector for efficient allelic replacement in naturally nontransformable, low-GC-content, gram-positive bacteria. *Applied and Environmental Microbiology*, *70*(11), 6887–6891. https://doi.org/10.1128/AEM.70.11.6887-6891.2004

Atilano, M. L., Pereira, P. M., Yates, J., Reed, P., Veiga, H., Pinho, M. G., & Filipe, S. R. (2010). Teichoic acids are temporal and spatial regulators of peptidoglycan cross-linking in Staphylococcus aureus. *Proceedings of the National Academy of Sciences of the United States of America*, *107*(44), 18991–18996. https://doi.org/10.1073/pnas.1004304107

Barthe, P., Mukamolova, G. V., Roumestand, C., & Cohen-Gonsaud, M. (2010). The Structure of PknB Extracellular PASTA Domain from Mycobacterium tuberculosis Suggests a Ligand-Dependent Kinase Activation. *Structure*, *18*(5), 606–615. https://doi.org/10.1016/j.str.2010.02.013

Bernardo-García, N., Mahasenan, K. V., Batuecas, M. T., Lee, M., Hesek, D., Petráčková, D., Doubravová, L., Branny, P., Mobashery, S., & Hermoso, J. A. (2018). Allostery, Recognition of Nascent Peptidoglycan, and Cross-linking of the Cell Wall by the Essential Penicillin-Binding Protein 2x of Streptococcus pneumoniae. *ACS Chemical Biology*, *13*(3), 694–702. https://doi.org/10.1021/acschembio.7b00817

Berrow, N. S., Alderton, D., & Owens, R. J. (2009). The precise engineering of expression vectors using high-throughput In-Fusion PCR cloning. *Methods in Molecular Biology (Clifton, N.J.)*, *498*, 75–90. https://doi.org/10.1007/978-1-59745-196-3_5

Berti, A. D., Sakoulas, G., Nizet, V., Tewhey, R., & Rose, W. E. (2013). β-Lactam Antibiotics Targeting PBP1 Selectively Enhance Daptomycin Activity against

Methicillin-Resistant Staphylococcus aureus. *Antimicrobial Agents and Chemotherapy*, *57*(10), 5005–5012. https://doi.org/10.1128/AAC.00594-13

Bertsche, U., Kast, T., Wolf, B., Fraipont, C., Aarsman, M. E. G., Kannenberg, K., von Rechenberg, M., Nguyen-Distèche, M., den Blaauwen, T., Höltje, J.-V., & Vollmer, W. (2006). Interaction between two murein (peptidoglycan) synthases, PBP3 and PBP1B, in Escherichia coli. *Molecular Microbiology*, *61*(3), 675–690. https://doi.org/10.1111/j.1365-2958.2006.05280.x

Bottomley, A. L., Kabli, A. F., Hurd, A. F., Turner, R. D., Garcia-Lara, J., & Foster, S. J. (2014). Staphylococcus aureus DivIB is a peptidoglycan-binding protein that is required for a morphological checkpoint in cell division. *Molecular Microbiology*. https://doi.org/10.1111/mmi.12813

Bunkóczi, G., & Read, R. J. (2011). Improvement of molecular-replacement models with Sculptor. *Acta Crystallographica. Section D, Biological Crystallography*, *67*(Pt 4), 303–312. https://doi.org/10.1107/S0907444910051218

Calvanese, L., Falcigno, L., Squeglia, F., D'Auria, G., & Berisio, R. (2017). Structural and dynamic features of PASTA domains with different functional roles. *Journal of Biomolecular Structure and Dynamics*, *35*(10), 2293–2300. https://doi.org/10.1080/07391102.2016.1217274

Campbell, J., Singh, A. K., Santa Maria, J. P., Kim, Y., Brown, S., Swoboda, J. G., Mylonakis, E., Wilkinson, B. J., & Walker, S. (2011). Synthetic lethal compound combinations reveal a fundamental connection between wall teichoic acid and peptidoglycan biosyntheses in Staphylococcus aureus. *ACS Chemical Biology*, *6*(1), 106–116. https://doi.org/10.1021/cb100269f

Chen, V. B., Arendall, W. B., Headd, J. J., Keedy, D. A., Immormino, R. M., Kapral, G. J., Murray, L. W., Richardson, J. S., & Richardson, D. C. (2010). MolProbity: All-atom

structure validation for macromolecular crystallography. *Acta Crystallographica. Section D, Biological Crystallography*, *66*(Pt 1), 12–21. https://doi.org/10.1107/S0907444909042073

Cho, H., Wivagg, C. N., Kapoor, M., Barry, Z., Rohs, P. D. A., Suh, H., Marto, J. A., Garner, E. C., & Bernhardt, T. G. (2016). Bacterial cell wall biogenesis is mediated by SEDS and PBP polymerase families functioning semi-autonomously. *Nature Microbiology*, *1*(10), 1–8. https://doi.org/10.1038/nmicrobiol.2016.172

Cooper, E. L., García-Lara, J., & Foster, S. J. (2009). YsxC, an essential protein in Staphylococcus aureus crucial for ribosome assembly/stability. *BMC Microbiology*, *9*, 266. https://doi.org/10.1186/1471-2180-9-266

Emsley, P., Lohkamp, B., Scott, W. G., & Cowtan, K. (2010). Features and development of Coot. *Acta Crystallographica. Section D, Biological Crystallography*, *66*(Pt 4), 486–501. https://doi.org/10.1107/S0907444910007493

Erster, O., & Liscovitch, M. (2010). A modified inverse PCR procedure for insertion, deletion, or replacement of a DNA fragment in a target sequence and its application in the ligand interaction scan method for generation of ligand-regulated proteins. *Methods in Molecular Biology (Clifton, N.J.)*, *634*, 157–174. https://doi.org/10.1007/978-1-60761-652-8_12

Evans, P. R., & Murshudov, G. N. (2013). How good are my data and what is the resolution? *Acta Crystallographica. Section D, Biological Crystallography*, *69*(Pt 7), 1204–1214. https://doi.org/10.1107/S0907444913000061

Farha, M. A., Leung, A., Sewell, E. W., D'Elia, M. A., Allison, S. E., Ejim, L., Pereira, P. M., Pinho, M. G., Wright, G. D., & Brown, E. D. (2013). Inhibition of WTA synthesis blocks the cooperative action of PBPs and sensitizes MRSA to β-lactams. *ACS Chemical Biology*, *8*(1), 226–233. https://doi.org/10.1021/cb300413m

1119 Fey, P. D., Endres, J. L., Yajjala, V. K., Widhelm, T. J., Boissy, R. J., Bose, J. L., & Bayles,
1120 K. W. (2013). A genetic resource for rapid and comprehensive phenotype screening
1121 of nonessential Staphylococcus aureus genes. *MBio*, *4*(1), e00537-00512.
1122 https://doi.org/10.1128/mBio.00537-12
1123 García-Lara, J., Weihs, F., Ma, X., Walker, L., Chaudhuri, R. R., Kasturiarachchi, J.,
1124 Crossley, H., Golestanian, R., & Foster, S. J. (2015). Supramolecular structure in the
1125 membrane of Staphylococcus aureus. *Proceedings of the National Academy of*
1126 *Sciences*, *112*(51), 15725–15730. https://doi.org/10.1073/pnas.1509557112
1127 Gibson, D. G., Young, L., Chuang, R.-Y., Venter, J. C., Hutchison, C. A., & Smith, H. O.
1128 (2009). Enzymatic assembly of DNA molecules up to several hundred kilobases.
1129 *Nature Methods*, *6*(5), 343–345. https://doi.org/10.1038/nmeth.1318
1130 Holm, L. (2020). DALI and the persistence of protein shape. *Protein Science: A Publication*
1131 *of the Protein Society*, *29*(1), 128–140. https://doi.org/10.1002/pro.3749
1132 Horsburgh, M. J., Aish, J. L., White, I. J., Shaw, L., Lithgow, J. K., & Foster, S. J. (2002). σB
1133 Modulates Virulence Determinant Expression and Stress Resistance: Characterization
1134 of a Functional rsbU Strain Derived from Staphylococcus aureus 8325-4. *Journal of*
1135 *Bacteriology*, *184*(19), 5457–5467. https://doi.org/10.1128/JB.184.19.5457-
1136 5467.2002
1137 Hudson, K. L., Bartlett, G. J., Diehl, R. C., Agirre, J., Gallagher, T., Kiessling, L. L., &
1138 Woolfson, D. N. (2015). Carbohydrate-Aromatic Interactions in Proteins. *Journal of*
1139 *the American Chemical Society*, *137*(48), 15152–15160.
1140 https://doi.org/10.1021/jacs.5b08424
1141 Hutter, J. L., & Bechhoefer, J. (1993). Calibration of atomic-force microscope tips. *Review of*
1142 *Scientific Instruments*, *64*(7), 1868–1873. https://doi.org/10.1063/1.1143970

1143 Kabsch, W. (2010). XDS. *Acta Crystallographica. Section D, Biological Crystallography*,
1144 *66*(Pt 2), 125–132. https://doi.org/10.1107/S0907444909047337
1145 Karimova, G., Ullmann, A., & Ladant, D. (2001). Protein-protein interaction between
1146 Bacillus stearothermophilus tyrosyl-tRNA synthetase subdomains revealed by a
1147 bacterial two-hybrid system. *Journal of Molecular Microbiology and Biotechnology*,
1148 *3*(1), 73–82.
1149 Kreiswirth, B. N., Löfdahl, S., Betley, M. J., O'Reilly, M., Schlievert, P. M., Bergdoll, M. S.,
1150 & Novick, R. P. (1983). The toxic shock syndrome exotoxin structural gene is not
1151 detectably transmitted by a prophage. *Nature*, *305*(5936), 709–712.
1152 https://doi.org/10.1038/305709a0
1153 Krissinel, E., & Henrick, K. (2007). Inference of macromolecular assemblies from crystalline
1154 state. *Journal of Molecular Biology*, *372*(3), 774–797.
1155 https://doi.org/10.1016/j.jmb.2007.05.022
1156 Kuru, E., Radkov, A., Meng, X., Egan, A., Alvarez, L., Dowson, A., Booher, G., Breukink,
1157 E., Roper, D. I., Cava, F., Vollmer, W., Brun, Y., & VanNieuwenhze, M. S. (2019).
1158 Mechanisms of Incorporation for D-Amino Acid Probes That Target Peptidoglycan
1159 Biosynthesis. *ACS Chemical Biology*, *14*(12), 2745–2756.
1160 https://doi.org/10.1021/acschembio.9b00664
1161 Lee, C. Y., Buranen, S. L., & Ye, Z. H. (1991). Construction of single-copy integration
1162 vectors for Staphylococcus aureus. *Gene*, *103*(1), 101–105.
1163 https://doi.org/10.1016/0378-1119(91)90399-v
1164 Liebschner, D., Afonine, P. V., Baker, M. L., Bunkóczi, G., Chen, V. B., Croll, T. I., Hintze,
1165 B., Hung, L. W., Jain, S., McCoy, A. J., Moriarty, N. W., Oeffner, R. D., Poon, B. K.,
1166 Prisant, M. G., Read, R. J., Richardson, J. S., Richardson, D. C., Sammito, M. D.,
1167 Sobolev, O. V., … Adams, P. D. (2019). Macromolecular structure determination

using X-rays, neutrons and electrons: Recent developments in Phenix. *Acta Crystallographica. Section D, Structural Biology*, *75*(Pt 10), 861–877. https://doi.org/10.1107/S2059798319011471

Loskill, P., Pereira, P. M., Jung, P., Bischoff, M., Herrmann, M., Pinho, M. G., & Jacobs, K. (2014). Reduction of the peptidoglycan crosslinking causes a decrease in stiffness of the Staphylococcus aureus cell envelope. *Biophysical Journal*, *107*(5), 1082–1089. https://doi.org/10.1016/j.bpj.2014.07.029

Lund, V. A., Wacnik, K., Turner, R. D., Cotterell, B. E., Walther, C. G., Fenn, S. J., Grein, F., Wollman, A. J., Leake, M. C., Olivier, N., Cadby, A., Mesnage, S., Jones, S., & Foster, S. J. (2018). Molecular coordination of Staphylococcus aureus cell division. *ELife*, *7*, e32057. https://doi.org/10.7554/eLife.32057

Maurer, P., Todorova, K., Sauerbier, J., & Hakenbeck, R. (2012). Mutations in Streptococcus pneumoniae penicillin-binding protein 2x: Importance of the C-terminal penicillin-binding protein and serine/threonine kinase-associated domains for beta-lactam binding. *Microbial Drug Resistance (Larchmont, N.Y.)*, *18*(3), 314–321. https://doi.org/10.1089/mdr.2012.0022

McCoy, A. J., Grosse-Kunstleve, R. W., Adams, P. D., Winn, M. D., Storoni, L. C., & Read, R. J. (2007). Phaser crystallographic software. *Journal of Applied Crystallography*, *40*(Pt 4), 658–674. https://doi.org/10.1107/S0021889807021206

Meeske, A. J., Riley, E. P., Robins, W. P., Uehara, T., Mekalanos, J. J., Kahne, D., Walker, S., Kruse, A. C., Bernhardt, T. G., & Rudner, D. Z. (2016). SEDS proteins are a widespread family of bacterial cell wall polymerases. *Nature*, *537*(7622), 634–638. https://doi.org/10.1038/nature19331

Mir, M., Asong, J., Li, X., Cardot, J., Boons, G.-J., & Husson, R. N. (2011). The Extracytoplasmic Domain of the Mycobacterium tuberculosis Ser/Thr Kinase PknB

Binds Specific Muropeptides and Is Required for PknB Localization. *PLOS Pathogens*, *7*(7), e1002182. https://doi.org/10.1371/journal.ppat.1002182

Morales Angeles, D., Macia-Valero, A., Bohorquez, L. C., & Scheffers, D.-J. (2020). The PASTA domains of Bacillus subtilis PBP2B strengthen the interaction of PBP2B with DivIB. *Microbiology (Reading, England)*, *166*(9), 826–836. https://doi.org/10.1099/mic.0.000957

Neuhaus, F. C., & Baddiley, J. (2003). A continuum of anionic charge: Structures and functions of D-alanyl-teichoic acids in gram-positive bacteria. *Microbiology and Molecular Biology Reviews: MMBR*, *67*(4), 686–723. https://doi.org/10.1128/mmbr.67.4.686-723.2003

Novick, R. P., & Morse, S. I. (1967). In vivo transmission of drug resistance factors between strains of Staphylococcus aureus. *The Journal of Experimental Medicine*, *125*(1), 45–59. https://doi.org/10.1084/jem.125.1.45

Panchal, V. V., Griffiths, C., Mosaei, H., Bilyk, B., Sutton, J. A. F., Carnell, O. T., Hornby, D. P., Green, J., Hobbs, J. K., Kelley, W. L., Zenkin, N., & Foster, S. J. (2020). Evolving MRSA: High-level β-lactam resistance in Staphylococcus aureus is associated with RNA Polymerase alterations and fine tuning of gene expression. *PLoS Pathogens*, *16*(7), e1008672. https://doi.org/10.1371/journal.ppat.1008672

Pasquina-Lemonche, L., Burns, J., Turner, R. D., Kumar, S., Tank, R., Mullin, N., Wilson, J. S., Chakrabarti, B., Bullough, P. A., Foster, S. J., & Hobbs, J. K. (2020). The architecture of the Gram-positive bacterial cell wall. *Nature*, *582*(7811), 294–297. https://doi.org/10.1038/s41586-020-2236-6

Pereira, S. F. F., Henriques, A. O., Pinho, M. G., de Lencastre, H., & Tomasz, A. (2007). Role of PBP1 in cell division of Staphylococcus aureus. *Journal of Bacteriology*, *189*(9), 3525–3531. https://doi.org/10.1128/JB.00044-07

1218 Pereira, S. F. F., Henriques, A. O., Pinho, M. G., de Lencastre, H., & Tomasz, A. (2009).
1219 Evidence for a dual role of PBP1 in the cell division and cell separation of
1220 Staphylococcus aureus. *Molecular Microbiology*, *72*(4), 895–904.
1221 https://doi.org/10.1111/j.1365-2958.2009.06687.x
1222 Pinho, M. G., de Lencastre, H., & Tomasz, A. (2001). An acquired and a native penicillin-
1223 binding protein cooperate in building the cell wall of drug-resistant staphylococci.
1224 *Proceedings of the National Academy of Sciences of the United States of America*,
1225 *98*(19), 10886–10891. https://doi.org/10.1073/pnas.191260798
1226 Pinho, M. G., & Errington, J. (2005). Recruitment of penicillin-binding protein PBP2 to the
1227 division site of Staphylococcus aureus is dependent on its transpeptidation substrates.
1228 *Molecular Microbiology*, *55*(3), 799–807. https://doi.org/10.1111/j.1365-
1229 2958.2004.04420.x
1230 Pinho, M. G., Filipe, S. R., de Lencastre, H., & Tomasz, A. (2001). Complementation of the
1231 essential peptidoglycan transpeptidase function of penicillin-binding protein 2 (PBP2)
1232 by the drug resistance protein PBP2A in Staphylococcus aureus. *Journal of*
1233 *Bacteriology*, *183*(22), 6525–6531. https://doi.org/10.1128/JB.183.22.6525-
1234 6531.2001
1235 Pinho, M. G., Kjos, M., & Veening, J.-W. (2013). How to get (a)round: Mechanisms
1236 controlling growth and division of coccoid bacteria. *Nature Reviews. Microbiology*,
1237 *11*(9), 601–614. https://doi.org/10.1038/nrmicro3088
1238 Reed, P., Atilano, M. L., Alves, R., Hoiczyk, E., Sher, X., Reichmann, N. T., Pereira, P. M.,
1239 Roemer, T., Filipe, S. R., Pereira-Leal, J. B., Ligoxygakis, P., & Pinho, M. G. (2015).
1240 Staphylococcus aureus Survives with a Minimal Peptidoglycan Synthesis Machine
1241 but Sacrifices Virulence and Antibiotic Resistance. *PLoS Pathogens*, *11*(5),
1242 e1004891. https://doi.org/10.1371/journal.ppat.1004891

1243 Reichmann, N. T., Tavares, A. C., Saraiva, B. M., Jousselin, A., Reed, P., Pereira, A. R.,
1244 Monteiro, J. M., Sobral, R. G., VanNieuwenhze, M. S., Fernandes, F., & Pinho, M. G.
1245 (2019). SEDS-bPBP pairs direct lateral and septal peptidoglycan synthesis in
1246 Staphylococcus aureus. *Nature Microbiology*, *4*(8), 1368–1377.
1247 https://doi.org/10.1038/s41564-019-0437-2
1248 Ruggiero, A., Squeglia, F., Marasco, D., Marchetti, R., Molinaro, A., & Berisio, R. (2011).
1249 X-ray structural studies of the entire extracellular region of the serine/threonine kinase
1250 PrkC from Staphylococcus aureus. *The Biochemical Journal*, *435*(1), 33–41.
1251 https://doi.org/10.1042/BJ20101643
1252 Sader, J. E., Borgani, R., Gibson, C. T., Haviland, D. B., Higgins, M. J., Kilpatrick, J. I., Lu,
1253 J., Mulvaney, P., Shearer, C. J., Slattery, A. D., Thorén, P.-A., Tran, J., Zhang, H.,
1254 Zhang, H., & Zheng, T. (2016). A virtual instrument to standardise the calibration of
1255 atomic force microscope cantilevers. *Review of Scientific Instruments*, *87*(9), 093711.
1256 https://doi.org/10.1063/1.4962866
1257 Sambrook, J., Fritsch, E. F., & Maniatis, T. (1989). Molecular cloning: A laboratory manual.
1258 *Molecular Cloning: A Laboratory Manual.*, *Ed. 2*.
1259 https://www.cabdirect.org/cabdirect/abstract/19901616061
1260 Saraiva, B. M., Sorg, M., Pereira, A. R., Ferreira, M. J., Caulat, L. C., Reichmann, N. T., &
1261 Pinho, M. G. (2020). Reassessment of the distinctive geometry of Staphylococcus
1262 aureus cell division. *Nature Communications*, *11*(1), 4097.
1263 https://doi.org/10.1038/s41467-020-17940-9
1264 Schenk, S., & Laddaga, R. A. (1992). Improved method for electroporation of
1265 Staphylococcus aureus. *FEMS Microbiology Letters*, *73*(1–2), 133–138.
1266 https://doi.org/10.1016/0378-1097(92)90596-g

1267 Schneider, T., & Sahl, H.-G. (2010). An oldie but a goodie—Cell wall biosynthesis as
1268 antibiotic target pathway. *International Journal of Medical Microbiology: IJMM*,
1269 *300*(2–3), 161–169. https://doi.org/10.1016/j.ijmm.2009.10.005
1270 Shah, I. M., Laaberki, M.-H., Popham, D. L., & Dworkin, J. (2008). A Eukaryotic-like
1271 Ser/Thr Kinase Signals Bacteria to Exit Dormancy in Response to Peptidoglycan
1272 Fragments. *Cell*, *135*(3), 486–496. https://doi.org/10.1016/j.cell.2008.08.039
1273 Silhavy, T. J., Kahne, D., & Walker, S. (2010). The bacterial cell envelope. *Cold Spring*
1274 *Harbor Perspectives in Biology*, *2*(5), a000414.
1275 https://doi.org/10.1101/cshperspect.a000414
1276 Squeglia, F., Marchetti, R., Ruggiero, A., Lanzetta, R., Marasco, D., Dworkin, J., Petoukhov,
1277 M., Molinaro, A., Berisio, R., & Silipo, A. (2011). Chemical Basis of Peptidoglycan
1278 Discrimination by PrkC, a Key Kinase Involved in Bacterial Resuscitation from
1279 Dormancy. *Journal of the American Chemical Society*, *133*(51), 20676–20679.
1280 https://doi.org/10.1021/ja208080r
1281 Srisuknimit, V., Qiao, Y., Schaefer, K., Kahne, D., & Walker, S. (2017). Peptidoglycan
1282 Cross-Linking Preferences of Staphylococcus aureus Penicillin-Binding Proteins
1283 Have Implications for Treating MRSA Infections. *Journal of the American Chemical*
1284 *Society*, *139*(29), 9791–9794. https://doi.org/10.1021/jacs.7b04881
1285 Steele, V. R., Bottomley, A. L., Garcia-Lara, J., Kasturiarachchi, J., & Foster, S. J. (2011).
1286 Multiple essential roles for EzrA in cell division of Staphylococcus aureus. *Molecular*
1287 *Microbiology*, *80*(2), 542–555. https://doi.org/10.1111/j.1365-2958.2011.07591.x
1288 Straume, D., Piechowiak, K. W., Olsen, S., Stamsås, G. A., Berg, K. H., Kjos, M.,
1289 Heggenhougen, M. V., Alcorlo, M., Hermoso, J. A., & Håvarstein, L. S. (2020). Class
1290 A PBPs have a distinct and unique role in the construction of the pneumococcal cell

wall. *Proceedings of the National Academy of Sciences of the United States of America*, *117*(11), 6129–6138. https://doi.org/10.1073/pnas.1917820117

Studier, F. W., & Moffatt, B. A. (1986). Use of bacteriophage T7 RNA polymerase to direct selective high-level expression of cloned genes. *Journal of Molecular Biology*, *189*(1), 113–130. https://doi.org/10.1016/0022-2836(86)90385-2

Su, H.-N., Li, K., Zhao, L.-S., Yuan, X.-X., Zhang, M.-Y., Liu, S.-M., Chen, X.-L., Liu, L.-N., & Zhang, Y.-Z. (2020). Structural Visualization of Septum Formation in Staphylococcus warneri Using Atomic Force Microscopy. *Journal of Bacteriology*, *202*(19). https://doi.org/10.1128/JB.00294-20

Sutton, J. A. F., Carnell, O. T., Lafage, L., Gray, J., Biboy, J., Gibson, J. F., Pollitt, E. J. G., Tazoll, S. C., Turnbull, W., Hajdamowicz, N. H., Salamaga, B., Pidwill, G. R., Condliffe, A. M., Renshaw, S. A., Vollmer, W., & Foster, S. J. (2021). Staphylococcus aureus cell wall structure and dynamics during host-pathogen interaction. *PLoS Pathogens*, *17*(3), e1009468. https://doi.org/10.1371/journal.ppat.1009468

Swoboda, J. G., Campbell, J., Meredith, T. C., & Walker, S. (2010). Wall teichoic acid function, biosynthesis, and inhibition. *Chembiochem: A European Journal of Chemical Biology*, *11*(1), 35–45. https://doi.org/10.1002/cbic.200900557

Taguchi, A., Welsh, M. A., Marmont, L. S., Lee, W., Sjodt, M., Kruse, A. C., Kahne, D., Bernhardt, T. G., & Walker, S. (2019). FtsW is a peptidoglycan polymerase that is functional only in complex with its cognate penicillin-binding protein. *Nature Microbiology*, *4*(4), 587–594. https://doi.org/10.1038/s41564-018-0345-x

Turner, R. D., Ratcliffe, E. C., Wheeler, R., Golestanian, R., Hobbs, J. K., & Foster, S. J. (2010). Peptidoglycan architecture can specify division planes in Staphylococcus aureus. *Nature Communications*, *1*, 26. https://doi.org/10.1038/ncomms1025

1316 Turner, R. D., Vollmer, W., & Foster, S. J. (2014). Different walls for rods and balls: The
1317 diversity of peptidoglycan. *Molecular Microbiology*, *91*(5), 862–874.
1318 https://doi.org/10.1111/mmi.12513
1319 Typas, A., Banzhaf, M., Gross, C. A., & Vollmer, W. (2011). From the regulation of
1320 peptidoglycan synthesis to bacterial growth and morphology. *Nature Reviews.*
1321 *Microbiology*, *10*(2), 123–136. https://doi.org/10.1038/nrmicro2677
1322 Vollmer, W., Blanot, D., & de Pedro, M. A. (2008). Peptidoglycan structure and architecture.
1323 *FEMS Microbiology Reviews*, *32*(2), 149–167. https://doi.org/10.1111/j.1574-
1324 6976.2007.00094.x
1325 Weidenmaier, C., Peschel, A., Xiong, Y.-Q., Kristian, S. A., Dietz, K., Yeaman, M. R., &
1326 Bayer, A. S. (2005). Lack of wall teichoic acids in Staphylococcus aureus leads to
1327 reduced interactions with endothelial cells and to attenuated virulence in a rabbit
1328 model of endocarditis. *The Journal of Infectious Diseases*, *191*(10), 1771–1777.
1329 https://doi.org/10.1086/429692
1330 Winn, M. D., Ballard, C. C., Cowtan, K. D., Dodson, E. J., Emsley, P., Evans, P. R., Keegan,
1331 R. M., Krissinel, E. B., Leslie, A. G. W., McCoy, A., McNicholas, S. J., Murshudov,
1332 G. N., Pannu, N. S., Potterton, E. A., Powell, H. R., Read, R. J., Vagin, A., & Wilson,
1333 K. S. (2011). Overview of the CCP4 suite and current developments. *Acta*
1334 *Crystallographica. Section D, Biological Crystallography*, *67*(Pt 4), 235–242.
1335 https://doi.org/10.1107/S0907444910045749
1336 Yang, Y., Bhachech, N., & Bush, K. (1995). Biochemical comparison of imipenem,
1337 meropenem and biapenem: Permeability, binding to penicillin-binding proteins, and
1338 stability to hydrolysis by beta-lactamases. *The Journal of Antimicrobial*
1339 *Chemotherapy*, *35*(1), 75–84. https://doi.org/10.1093/jac/35.1.75

1340 Yeats, C., Finn, R. D., & Bateman, A. (2002). The PASTA domain: A beta-lactam-binding
1341 domain. *Trends in Biochemical Sciences*, *27*(9), 438. https://doi.org/10.1016/s0968-
1342 0004(02)02164-3
1343 Zapun, A., Contreras-Martel, C., & Vernet, T. (2008). Penicillin-binding proteins and beta-
1344 lactam resistance. *FEMS Microbiology Reviews*, *32*(2), 361–385.
1345 https://doi.org/10.1111/j.1574-6976.2007.00095.x
1346 Zhao, G., Meier, T. I., Kahl, S. D., Gee, K. R., & Blaszczak, L. C. (1999). BOCILLIN FL, a
1347 Sensitive and Commercially Available Reagent for Detection of Penicillin-Binding
1348 Proteins. *Antimicrobial Agents and Chemotherapy*, *43*(5), 1124–1128.
1349 Zhou, X., Halladin, D. K., Rojas, E. R., Koslover, E. F., Lee, T. K., Huang, K. C., & Theriot,
1350 J. A. (2015). Bacterial division. Mechanical crack propagation drives millisecond
1351 daughter cell separation in Staphylococcus aureus. *Science (New York, N.Y.)*,
1352 *348*(6234), 574–578. https://doi.org/10.1126/science.aaa1511
1353

Appendix Tables

Appendix Table 1. Strains used in this study

Name	Relevant genotype/Markers	Source
Staphylococcus aureus		
SH1000	Functional *rsbU*$^{+}$ derivative of *S. aureus* 8325-4	(Horsburgh et al., 2002)
VF17	SH1000 pGL485 (*lacI*); Cm^R	(Steele et al., 2011)
RN4220	Restriction deficient transformation recipient	(Kreiswirth et al., 1983)
CYL316	RN4220 pCL112Δ19	(Lee et al., 1991)
SJF4588	SH1000 *geh::*P*spac-pbp1*; Tet^R	This study
SJF5116	SH1000 *geh::*P*spac -pbp1* Δ*pbp1*; Tet^R	This study
SJF5275	SH1000 *geh::*P*spac -pbp1 pbp1*$_{\Delta PASTA}$; Tet^R	This study
SJF4590	SH1000 *geh::*P*spac -pbp1 pbp1** Tet^R, Cm^R	This study
Δ*pbp1*	SH1000 *geh::*P*spac -pbp1* Δ*pbp1 lacI*; Tet^R	This study
pbp1$_{\Delta PASTA}$	SH1000 *geh::*P*spac -pbp1 pbp1*$_{\Delta PASTA}$ *lacI*; Tet^R, Cm^R	This study
*pbp1**	SH1000 *geh::*P*spac -pbp1 pbp1* lacI*; Tet^R, Cm^R	This study
SJF5046	SH1000 *lysA::*p*mecA rpoB*^{H929Q}; Ery^R, Kan^R	(Panchal et al., 2020)
Δ*pbp1* p*mecA*	SH1000 *geh::*P*spac-pbp1* Δ*pbp1 lacI lysA::pmecA*; Tet^R, Cm^R, Ery^R	This study
*pbp1** p*mecA*	SH1000 *geh::*P*spac-pbp1 pbp1* lacI lysA::*p*mecA*; Tet^R, Cm^R, Ery^R	This study
MRSA Δ*pbp1*	SH1000 *geh::*P*spac-pbp1* Δ*pbp1 lacI lysA::*p*mecA rpoB*^{H929Q}; Tet^R, Cm^R, Ery^R, Kan^R	This study
MRSA *pbp1**	SH1000 *geh::*P*spac-pbp1 pbp1* lacI lysA::*p*mecA rpoB*^{H929Q}; Tet^R, Cm^R, Ery^R, Kan^R	This study
JGL227	SH1000 *ezrA-gfp*+; Ery^R	(Steele et al., 2011)
Δ*pbp1 ezrA-gfp*	SH1000 *geh::*P*spac-pbp1* Δ*pbp1 lacI ezrA-gfp*; Tet^R, Cm^R, Ery^R	This study
pbp1$_{\Delta PASTA}$ *ezrA-gfp*	SH1000 *geh::*P*spac-pbp1 pbp1*$_{\Delta PASTA}$ *lacI ezrA-gfp*; Tet^R, Cm^R, Ery^R	This study

pbp1 ezrA-gfp*	SH1000 *geh::*P*spac-pbp1 pbp1* lacI ezrA-gfp*; Tet^R, Cm^R, Ery^R	This study
NE420	JE2 *pbp3::Tn*; Ery^R	(Fey et al., 2013)
SH4421	SH1000 *pbp3::Tn*; Ery^R	This study
NE3004	RN4220 pKAN; Cm^R, Ery^R	(Fey et al., 2013)
SH4425	*pbp4::Tn*; Ery^R	(Lund et al., 2018)
SH5115	SH1000 *pbp4::kan*; Kan^R	This study
pbp3 pbp4 (SH5483)	*pbp3::Tn pbp4::kan*; Ery^R ,Kan^R,	This study
Δ*pbp1 pbp4*	SH1000 *geh::*P*spac-pbp1* Δ*pbp1 lacI pbp4::Tn*; Tet^R, Cm^R, Kan^R	This study
$pbp1_{\Delta PASTA}$ *pbp4*	SH1000 *geh::*P*spac-pbp1* $pbp1_{\Delta PASTA}$ *lacI pbp4::Tn*; Tet^R, Cm^R, Kan^R	This study
pbp1 pbp4*	SH1000 *geh::*P*spac-pbp1 pbp1* lacI pbp4::Tn*; Tet^R, Cm^R, Kan^R	This study
tarO	SH1000 Δ*tarO::ery*; Ery^R	Constructed by Dr B. Salamaga (University of Sheffield)
tarO tarO+	SA113 Δ*tarO::ery* pUC1-*tarO* ; Ery^R, Cm^R	Constructed by Dr B. Salamaga (University of Sheffield)
Δ*pbp1 tarO*	SH1000 *geh::*P*spac-pbp1* Δ*pbp1 lacI* Δ*tarO::ery*; Tet^R, Cm^R, Ery^R	This study
$pbp1_{\Delta PASTA}$ *tarO*	SH1000 *geh::*P*spac-pbp1* $pbp1_{\Delta PASTA}$ *lacI* Δ*tarO::ery*; Tet^R, Cm^R, Ery^R	This study
pbp1 tarO*	SH1000 *geh::*P*spac-pbp1 pbp1* lacI* Δ*tarO::ery*; Tet^R, Cm^R, Ery^R	This study
Escherichia coli		
NEB5α	*fhuA2 (argF-lacZ)U169 phoA glnV44 80 (lacZ)*M15 *gyrA96 recA1 relA1 endA1 thi-1 hsdR17*	New England Biolabs
BTH101	*F⁻, cya-99, araD139, galE15, galK16, rpsL1, hsdR2, mcrA1, mcrB1*	(Karimova et al., 2001)
Rosetta (DE3)	*F- ompT hsdS*$_B$(r_B- m_B-) *gal dcm* (DE3) pRARE (Cm^R)	Novagen
BL21(DE3)	F⁻ *omp*T *hsd*S_B (r_B⁻, m_B⁻) *gal dcm* (DE3)	(Studier & Moffatt, 1986)

1356

1357 **Appendix Table 2. Plasmids used in this study**

Name	Characteristics	Source
pCQ11-FtsZ-SNAP	pCQ11 derivative containing *ftsZ-snap* under P*spac*; Amp^R, Ery^R	(Lund et al., 2018)
pKASBAR	pUC18 containing *attP* and tetracycline cassette; Amp^R, Tet^R	(Bottomley et al., 2014)
pKB-P*spac-pbp1*	pKASBAR containing *S. aureus pbp1* under P*spac*; Amp^R, Tet^R	This study
pMAD	*E. coli-S. aureus* shuttle vector with temperature-sensitive origin of replication in *S. aureus* and constitutively produced thermostable β-galactosidase encoded by *bgaB*; Amp^R, Ery^R	(Arnaud et al., 2004)
pMAD-Δ*pbp1*	pMAD containing a deletion cassette for *S. aureus pbp1*; Amp^R, Ery^R	This study
pMAD-*pbp1*$_{\Delta PASTA}$	pMAD containing a deletion cassette for *S. aureus pbp1* PASTA domains; Amp^R, Ery^R	This study
pMAD-*pbp1**	pMAD containing a cassette for introduction of a point mutation (S314A) in the active site *S. aureus pbp1*; Amp^R, Ery^R	This study
pGL485	*E. coli-S. aureus* shuttle vector carrying *E. coli lacI* gene under the control of a constitutive promoter; $Spec^R$, Cam^R	(Cooper et al., 2009)
T18 (pUT18C)	Derivative of high copy-number pUC19, carrying gene encoding amino acids 225 to 399 of CyaA (T18 fragment); Amp^R	(Karimova et al., 2001)
T18-zip (pUT18C-zip)	pUT18C coding for the leucine zipper region of the GCN4 yeast protein. Positive control; Amp^R	(Karimova et al., 2001)
EzrA-T18 (pVF32)	pUT18(Karimova et al., 2001) containing T18 fused in frame to the 3′ end of *S. aureus ezrA*; Amp^R	(Steele et al., 2011)
T18-PBP2 (pGL547)	pUT18C containing T18 fused in frame to the 5′ end of *S. aureus pbp2*; Amp^R	(Steele et al., 2011)
T18-DivIC (pGL564)	pUT18C containing T18 fused in frame to the 5′ end of *S. aureus divIC*; Amp^R	(Steele et al., 2011)
T18-DivIB (pGL544)	pUT18C containing T18 fused in frame to the 5′ end of *S. aureus divIB*; Amp^R	(Steele et al., 2011)
T18-FtsW (pALB6)	pUT18C containing T18 fused in frame to the 5′ end of *S. aureus ftsW*; Amp^R	(Steele et al., 2011)
T25 (pKT25)	Derivative of low copy-number pSU40, carrying the first 224 amino acids of *B. subtilis* CyaA (T25 fragment); Kan^R	(Karimova et al., 2001)

T25-zip (pKT25-zip)	pKT25 coding for the leucine zipper region of the GCN4 yeast protein. Positive control; Kan^R	(Karimova et al., 2001)
T25-PBP1 (pGL550)	pKT25 containing T25 fused in frame to the 5′ end of *S. aureus pbp1*; Kan^R	(Steele et al., 2011)
T25-PBP1$_{\Delta PASTA}$	pKT25 containing T25 fused in frame to the 5′ end of *S. aureus pbp1*$_{\Delta PASTA}$ (M1-S595); Kan^R	This study
pOPINRSF	*kan* P_{T7} *lacI*; Kan^R	(Berrow et al., 2009)
pVR01	*kan* P_{T7} *pbp1 lacI*; pOPINRSF derivative for overexpression of full length *S. aureus* PBP1 (1-744); Kan^R	This study
pVR02	*kan* P_{T7} *pbp1*(*37-744*) *lacI*; pOPINRSF derivative for overexpression of *Sa*PBP1 (37-744); Kan^R	This study.
pVR03	*kan* P_{T7} *pbp1**(*37-744*: S314A) *lacI*; pOPINRSF derivative for overexpression of *Sa*PBP1* (37-744); Kan^R	This study
pVR04	*kan* P_{T7} *pbp1*(*37-595*) *lacI*; pOPINRSF derivative for overexpression of *Sa*PBP1$_{\Delta PASTA}$(37-595); Kan^R	This study
pVR06	*kan* P_{T7} *pbp1*(*595-744*) *lacI*; pOPINRSF derivative for overexpression of *Sa*PASTA$_{PBP1}$ (595-744); Kan^R	This study
pOPINJB	*bla* P_{T7} *lacI*; Amp^R	(Berrow et al., 2009)
pSA50	pOPINJB derivative for overexpression of sPBP1A-BAP; Amp^R	This study

1358

1359 **Appendix Table 3. Oligonucleotides used in this study**

Name	5′-3′ oligonucleotide sequence
pCQ-pbp1-F	AGAAGGAGATATACATATGGCTTGAGAACGATAATGTAAAG
pCQ-pbp1-F	TATTATGCATTTAGAATAGGTTAGTCCGACTTATCCTTG
pKB-Pspac-pbp1-F	CCTTTTTTTGCCCCGGGATCCGCAAAAAGTTGTTGACTTTATC
pKB-Pspac-pbp1-R	CTATGACCATGATTACGAATTCTTAGTCCGACTTATCCTTG
pbp1-A	CCATGGTACCCGGGAGCTCGCACCATGACGCAACATTAG
pbp1-B	ATCCTTGTCATTAATTTTTTGCTTCGCC
pbp1-C	CAAAAAATTAATGACAAGGATAAGTCGGAC
pbp1-D	CCTCGCGTCGGGCGATATCGATCTCCCATAAACACTTTAGC
pbp1-E	CCATGGTACCCGGGAGCTCGAATTCTAAAAAACCTAGGCATG
pbp1-F	TATCCTTGTCAGATGTGTCATCTTTTGATTTAC
pbp1-G	TGACACATCTGACAAGGATAAGTCGGACTAAC
pbp1-H	GCGTCTGCAGAAGCTTCTAGTTAATGCACTCCAATCCATAAAC
pbp1*5′-F	CCATGGTACCCGGGAGCTCGAATTCAGTATACCGAAGCAACAACCAC
pbp1*5′-R	TTAAATGTTGCTCCAGGCTCGTATGTGTTTTG
pbp1*3′-F	GAGCCTGGAGCAACATTTAAATCAT ATGGGTTA
pbp1*3′-R	CCTCGCGTCGGGCGATATCGGATCCTTAGTCCGACTTATCCTTGTC
T25-pbp1-F	CTGCAGGGTCGACTCTAGAGATGGCGAAGCAAAAAATTAAAATTAAAAAAAATAAAATAG
T25-pbp1pasta-R	ACGTTGTAAAACGACGGCCGTTAAGATGTGTCATCTTTTGATTTACCTACATTTAAATATTTC
VR47F	AAGTTCTGTTTCAGGGCCCGGCGAAGCAGAAGATCAAGATTAAGAAAAAC
VR47R	ATGGTCTAGAAAGCTTTAATCGCTTTTATCCTTGTCGGTTTTGC
VR49F	ATGATTACCGGCCACAGCAAC
VR49R	CGGGCCCTGAAACAGAACTTCCAG
VR51	AACACCTATGAGCCGGGCGCCACCTTCAAAAGCTATGGTC
VR53	GAGCAAAGACGATACCAGCTAAGCGGAGTACAGCAAGG
VR57F	AGCAACGCGGAGTACAGCAAGGTGCCGGACGTTG

OPPF20018F	AAGTTCTGTTTCAGGGCCCGGCGAACGAGAAATACCTGGTTAAGAACGCGC
OPPF20018R	AGATGTCGTTCAGGCCATCGCTTTTATCCTTGTCGGTTTTGCTGTCGC

1360

1361 **Appendix Table 4. Crystallographic data**

	***Sa*PASTA$_{PBP1}$**
Data	
Resolution (Å)	1.78
Space group	$P2_12_12_1$
a, *b*, *c* (Å)	39.8, 81.4, 89.6
α, β, γ (°)	90, 90, 90
<I/σI>[a]	14.2 (2.0)
Completeness (%)[a]	99.9 (99.8)
Redundancy[a]	7.7 (6.7)
$R_{p.i.m}$ (%)[a]	3.0 (39.1)
R_{merge} (%)[a]	6.0 (66.0)
$CC_{1/2}$[a]	99.8 (92.3)
Refinement	
R_{work} (%)	18.7 %
R_{free} (%)[b]	21.0 %
No. of residues	Chain A: 116, Chain B: 117
No. of waters	123
Average *B*-factor (Å^2)	
Protein	Chain A: 45.1, Chain B: 48.0
Waters	47.6
R.m.s.d on ideal values	
Bond lengths (Å)	0.005
Bond angle (°)	0.755
Ramachandran	
Most favoured (%)	98.69
Additional allowed (%)	1.31
Outliers (%)	0.0
PDB ID	7O61

1362 [a]Values in parentheses are for the highest resolution shell.

1363 [b]For determination of R_{free}, 5 % of reflections were randomly selected before refinement.